

On a pair of interacting bubbles in planar Stokes flow

By DARREN CROWDY¹, SALEH TANVEER²
AND GIOVANI L. VASCONCELOS³

¹Department of Mathematics, Imperial College of Science, Technology and Medicine,
180 Queen's Gate, London, SW7 2AZ, UK

²Department of Mathematics, Ohio State University, W 18th Avenue, Columbus, OH 43210, USA

³Laboratório de Física Teórica e Computacional, Departamento de Física, Universidade
Federal de Pernambuco, 50670-901, Recife, Brazil

(Received 3 May 2004 and in revised form 11 April 2005)

This paper presents a combined numerical and analytical investigation into various problems involving two symmetric interacting constant-pressure bubbles evolving in two-dimensional Stokes flow. The bubbles have constant surface tension on their boundaries and are taken to be in an ambient straining flow. First, a novel numerical method based on conformal mappings is presented to compute the free-surface evolution. Then, a special class of time-evolving exact solutions to the problem is derived and used to check the numerical code. These solutions reveal that, for bubbles with shrinking area, a competition between the imposed strain and surface tension can lead to either a slit or a point as the limiting shape. Numerical solutions of fixed-area bubbles are then computed and reveal that when they are forced together by a straining flow, a thin lubrication layer forms. In the absence of surface tension, large-curvature regions develop at the bubble edges and these are smoothed out by capillary effects. Further, motivated by the viscous sintering application, a study of interaction effects on the pure surface-tension-driven shrinkage of circular bubbles is investigated and compared, in an appropriate limit, to a recently derived 'elliptical-pore model'.

1. Introduction

The study of bubbles evolving in slow viscous flows is of fundamental importance in many practical applications such as the rheology of emulsions and mixing in multi-phase systems. Since the early work of Taylor (1934) there has been much theoretical and experimental research. The reviews by Acrivos (1983), Rallison (1984) and Stone (1994) provide good surveys on the background to the problem.

This paper focuses on the two-dimensional problem. Concerning this case, Richardson (1968, 1973) made significant early contributions by uncovering exact solutions, using the methods of complex analysis, for a single steady bubble in an ambient Stokes flow. Theoretical study of the planar problem has experienced a revival in recent years owing to the realization that the mathematical approach admits a generalization that yields classes of exact solutions that are not simply steady but evolve in time. By the term 'exact solution' we refer to a solution for the free-boundary evolution which can be exactly reduced to the solution of a finite set of ordinary differential equations. Hopper (1990, 1991) found certain time-evolving solutions for

a fluid blob driven by surface tension. Antanovskii (1994a) found classes of solution for an incompressible bubble in a polynomially singular irrotational straining flow in the far-field. Tanveer & Vasconcelos (1995) derived exact solutions for a single bubble in an ambient linear shear/strain flow and considered the effect of shrinkage and expansion of bubble area on its dynamics. Later, Antanovskii (1996) combined the ideas of matched asymptotic expansions with an exact complex-variable solution for the flow around a bubble to make detailed comparisons with the experimental study performed by Taylor (1934) of a steady bubble in a four-roller mill device.

All these studies involve a single isolated bubble. It is natural to ask whether it is possible to find analogous exact solutions to the problem of multiple interacting bubbles. This is one of the questions which this paper seeks to address. The fluid region exterior to the bubbles in a multi-bubble configuration is necessarily multiply connected. The evidence that exact time-evolving solutions exist for the problem of multiply connected blobs of viscous fluid (Richardson 2000; Crowdy 2003b) renders the question of existence of exact solutions to multi-bubble problems even more tantalizing.

Concerning interacting bubbles in two-dimensional Stokes flow, a few analytical results already exist. The only exact solutions involving non-trivial bubble shapes appear to be those of Crowdy (2002) who identified a class of exact solutions for the problem of two steady bubbles in an ambient Stokes flow typical of that produced at the centre of a four-roller mill. The latter work generalizes the analysis of Antanovskii (1996) and Siegel (2000) who have studied single bubbles in the same class of ambient flows. For modelling multiple interacting bubbles (or ‘pores’), motivated by the application to viscous sintering (Brinker & Scherer 1990), Crowdy (2004) has proposed a simple ‘elliptical-pore model’ of a distribution of interacting bubbles shrinking under the effects of surface tension. The model is based on a generalization of the solutions of Tanveer & Vasconcelos (1995) to the case of an arbitrarily compressible bubble (Crowdy 2003a).

Despite being less realistic for physical applications, the planar problem is an important paradigm with the potential to allow tractable mathematical investigation. It can yield qualitative insights into the free-surface dynamics that are also likely to pertain in the three-dimensional case. Importantly, the planar problem also arises in various asymptotic limits of the three-dimensional problem. Cummings & Howell (1999) have exploited a slenderness assumption in their studies of long viscous fibres to reduce the three-dimensional equations to a sequence of weakly coupled quasi-two-dimensional problems. In the same vein, Howell & Siegel (2004) have shown that the problem of a long slender three-dimensional bubble in a straining flow can be decomposed into a collection of ‘cross-flow problems’ that can be solved explicitly, even in the non-axisymmetric case, using the planar solution methods of Tanveer & Vasconcelos (1995) and Antanovskii (1994a). Eggers, Lister & Stone (1999) have also made use of the planar exact solutions due to Hopper (1990) in their studies of certain limits of the three-dimensional problem of droplet coalescence.

This paper presents the results of our investigations of the two-bubble problem in the case where they are placed in an ambient linear straining flow with strain rate $\beta(t)$. In §2 and §3, the mathematical problem is presented in terms of a complex-variable formulation in which two Goursat functions $f(z, t)$ and $g(z, t)$ are introduced that are analytic in the fluid region. Section 4 describes a convenient parametrization of the bubble boundaries in terms of conformal mappings from an annulus in a pre-image ζ -plane. This conformal mapping formulation not only facilitates the devising of an effective numerical spectral method based on the Laurent expansion of the conformal

mapping (and the Goursat functions) in this annulus but also leads to the derivation of a special class of time-evolving exact solutions when a certain parameter $C(t)$ arising in the formulation vanishes. Unfortunately, if $C(t)$ vanishes it means there is a constraint between the imposed strain rate $\beta(t)$ and the evolution of the bubble area. Thus, for specified $\beta(t)$, the bubble area evolves in a manner determined by the solution itself and cannot be externally specified as is desirable in applications. Despite this circumstance, the exact solutions are mathematically significant, being non-trivial and time-evolving. They display interesting general properties and, importantly, can be used as a non-trivial check on the numerical calculations. Exact solutions demonstrate the fact that for shrinking bubbles, there is a competition between the imposed strain and surface tension that can lead to either a slit or a point as the limiting shape.

The numerical algorithm can compute the bubble evolution for any value of $C(t)$ and therefore without any constraints on the bubble area evolution. Indeed, for a given ambient straining flow it is found that $C(t)$ is determined by the condition imposed on the bubble area evolution. Calculations reveal that if two symmetric bubbles of fixed area are forced together by a straining flow, a thin lubrication layer forms. At the edges, high-curvature points develop in the absence of surface tension suggesting the eventual breakdown of the mathematical solution via the formation of cusps in the bubble boundaries. High-curvatures, as expected, are smoothed out in the presence of capillary effects resulting, at large times, in long flat bubbles with an extended lubrication layer between them. While Kropinski (2002) has recently developed efficient methods for time-evolving multiple bubbles in two dimensions that require $O(N)$ operations at each time step, the particular conformal-mapping-based method devised here is well-suited to deformed bubbles. This is because equally spaced points on $|\zeta|=1$ and $|\zeta|=\rho$ tends to concentrate more near the deformed regions of the bubbles.

Motivated by application to viscous sintering, we also extend the results of Hopper (1990). He studied isolated bubbles of circular, elliptical or hypotrochoidal shape driven purely by surface tension and was interested in how long it takes the bubbles to close up. An interesting question is how the presence of another neighbouring bubble can affect Hopper's results. In the two-bubble situation, we find that the presence of a neighbouring bubble can accelerate the time taken for an initially circular pore to shrink to zero area. When the bubbles are not too close together, the results of the numerical simulation are compared to a recently derived 'elliptical-pore model' due to Crowdy (2004) which is based on simple exact solutions.

2. The two-bubble problem

Consider an unbounded planar region of slow viscous fluid containing two bubbles as shown schematically in figure 1. Let the evolving fluid region exterior to the two bubbles be $D(t)$. Inertia is ignored so the fluid is assumed to be in the Stokes regime with an ambient (and possibly time-dependent) pressure $p_\infty(t)$ at infinity. The physical assumption inside the bubbles is that they are each at the same spatially constant pressure; without loss of generality, this can be taken to be zero.†

† This can be generalized to the case where an equation of state gives the pressure inside each bubble as a function of its area (e.g. the product of the bubble pressure with its area is a constant in the case of an ideal gas), as done for the single bubble case (Crowdy 2003). As long as the two bubbles have identical equations of state, the methodology given here extends to that case as well.

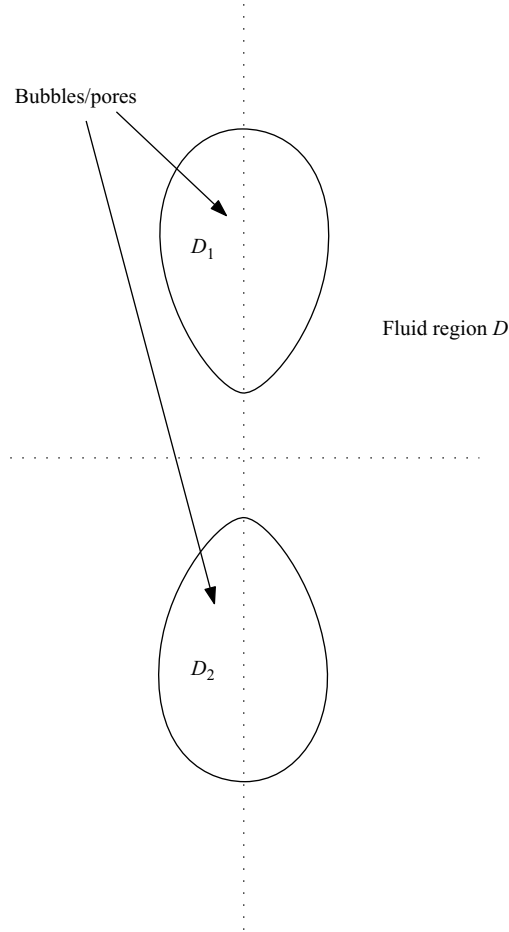


FIGURE 1. Schematic illustrating the flow configuration. The fluid region D is exterior to two bubbles (or ‘pores’) D_1 and D_2 . The two bubbles are reflectionally symmetric about both the x - and y -axes.

The Stokes flow outside the bubbles is incompressible. Introducing a stream function $\psi(x, y)$ such that

$$\mathbf{u} = (\psi_y, -\psi_x), \quad (2.1)$$

then it is well-known (see, for instance, Richardson 1968) that ψ satisfies the biharmonic equation in the fluid region, i.e.

$$\nabla^4 \psi = 0. \quad (2.2)$$

A uniform surface tension acts on the bubble boundaries, the coefficient of surface tension being the same for both. The equation of stress balance on each bubble boundary takes the form

$$-pn_j + 2\mu e_{jk}n_k = \sigma\kappa n_j, \quad (2.3)$$

where p is the fluid pressure, e_{jk} is the fluid rate-of-strain tensor, n_k is the k th component of normal vector \mathbf{n} , κ is the surface curvature and σ the coefficient of surface tension. The kinematic boundary condition on the interface is that the normal

velocity of the boundary, denoted V_n , is equal to the normal fluid velocity, i.e.

$$V_n = \mathbf{u} \cdot \mathbf{n}. \tag{2.4}$$

In the far-field, the flow is assumed to be that of a straining flow with (possibly time-dependent) strain rate $\beta(t)$, i.e.

$$(u, v) = (\beta(t)x, -\beta(t)y) + o(1). \tag{2.5}$$

We seek solutions to this quasi-steady free boundary problem in which the evolution of an initial two-bubble configuration is driven by both surface tension and the ambient straining flow. Of course, it must be assumed that the time derivative of $\beta(t)$ must be suitably small in order not to violate the assumption of the Stokes flow approximation.

It is assumed that the two bubbles are reflections of each other about the y -axis. They will also be taken to be reflectionally symmetric about the x -axis. See figure 1. The flow field will be assumed to have the same reflectional symmetries about both the x - and y -axes. It follows immediately that we must have

$$u(0, y) = 0, \quad v(x, 0) = 0. \tag{2.6}$$

Furthermore, since the vorticity ω is defined as

$$\omega \equiv \frac{\partial v}{\partial x} - \frac{\partial u}{\partial y} \tag{2.7}$$

it follows that

$$\omega(x, -y) = -\omega(x, y), \quad \omega(-x, y) = -\omega(x, y). \tag{2.8}$$

These relations imply that the vorticity must be zero on both the x - and y -axes.

3. Complex-variable formulation

We now reformulate the free boundary problem using complex-variable methods. The general solution of (2.2) in the fluid exterior to the two bubbles can be written, in terms of the usual complex variable $z = x + iy$ and its complex conjugate $\bar{z} = x - iy$, as

$$\psi = \text{Im}[\bar{z}f(z, t) + g(z, t)], \tag{3.1}$$

where $f(z, t)$ and $g(z, t)$ are analytic everywhere in the fluid region except at infinity where they have possible singular behaviour. The following relations can be established (Tanveer & Vasconcelos 1995):

$$\frac{p}{\mu} - i\omega = 4f'(z, t), \tag{3.2}$$

$$u + iv = -f(z) + z\bar{f}'(\bar{z}, t) + \bar{g}'(\bar{z}, t), \tag{3.3}$$

$$e_{11} + ie_{12} = z\bar{f}''(\bar{z}, t) + \bar{g}''(\bar{z}, t). \tag{3.4}$$

In the above, we define conjugate functions to be given by

$$\bar{h}(z) = \overline{h(\bar{z})}. \tag{3.5}$$

If there are no external forces on the bubbles then $f(z, t)$ will be single-valued in $D(t)$. On the other hand, if the area of the bubbles changes, $g(z, t)$ will in general not be single-valued, corresponding to sources or sinks in the bubbles.

It is convenient to non-dimensionalize velocities by σ/μ , pressure by σ/r_0 and length and time scales with r_0 and $r_0\mu/\sigma$ respectively, where r_0 is a length scale chosen so that the initial area of each bubble is πr_0^2 . With respect to this non-dimensionalization, the parameter $\beta(t)$ in (2.5) takes on the role of a capillary number giving the ratio of time scales associated with the ambient straining flow to that associated with surface tension effects.

Defining s to be the arclength traversed in a clockwise direction around the two bubble boundaries, it turns out (see, for example, Tanveer & Vasconcelos 1995) that the complex form of the stress conditions (2.3) can be integrated with respect to s to yield

$$f(z, t) + z\bar{f}'(\bar{z}, t) + \bar{g}'(\bar{z}, t) = -i\frac{z_s}{2} + \mathcal{A}_1(t), \tag{3.6}$$

$$f(z, t) + z\bar{f}'(\bar{z}, t) + \bar{g}'(\bar{z}, t) = -i\frac{z_s}{2} + \mathcal{A}_2(t) \tag{3.7}$$

where a subscript s denotes the derivative with respect to arclength, and $\mathcal{A}_1(t)$ and $\mathcal{A}_2(t)$ are functions of time arising in the spatial integration.

It has been established that the vorticity on the real and imaginary z -axes is zero. This implies, from (3.3), that $f'(z, t)$ is real on both axes. By integration along each axis, it is clear that, without loss of generality, we can choose $f(z, t)$ to be purely real on the real axis, and purely imaginary on the imaginary axis exterior to the bubble. It has also been established that $u + iv$ is purely real on the real axis and purely imaginary on the imaginary axis exterior to the bubbles. By (3.4), and the results just established for $f(z, t)$ and $f'(z, t)$, it follows that $g'(z, t)$ is real on the real axis and imaginary on the imaginary axis exterior to the bubbles. In summary, both $f(z, t)$ and $g'(z, t)$ are real on the real axis and imaginary on the imaginary axis exterior to the bubbles. In particular, we have

$$\bar{f}(z, t) = f(z, t) = -f(-z, t) \quad \text{and} \quad \bar{g}'(z, t) = g'(z, t) = -g'(-z, t), \tag{3.8}$$

so that

$$f(0, t) = g'(0, t) = 0. \tag{3.9}$$

The \mathcal{A}_1 and \mathcal{A}_2 appearing in (3.6) and (3.7) cannot be absorbed into the definitions of the functions $f(z, t)$ or $g'(z, t)$, without invalidating relations (3.2)–(3.4) and/or (3.9).

From (3.8) it follows that if

$$f(z, t) + z\bar{f}'(\bar{z}, t) + \bar{g}'(\bar{z}, t) = -\frac{iz_s}{2} + \mathcal{A}_1(t) \tag{3.10}$$

on the half-bubble boundary in the first quadrant, then since $[z_s]_{\text{fourth quad.}} = -[\bar{z}_s]_{\text{first quad.}}$, we have that

$$f(z, t) + z\bar{f}'(\bar{z}, t) + \bar{g}'(\bar{z}, t) = -\frac{iz_s}{2} + \mathcal{A}_2(t) \tag{3.11}$$

on the half-bubble in the fourth quadrant, with

$$\overline{\mathcal{A}_2(t)} = \mathcal{A}_1(t). \tag{3.12}$$

Using a similar argument for the first and third quadrants, it follows that

$$\mathcal{A}_1(t) = -\overline{\mathcal{A}_1(t)}. \tag{3.13}$$

Thus, $\mathcal{A}_1(t) = iC(t) = -\mathcal{A}_2(t)$ for some real $C(t)$.

It is assumed that there is some non-zero ambient pressure $p_\infty(t)$ at infinity. This implies that

$$f'(z, t) \sim \frac{p_\infty(t)}{4} + O(1/z^2) \quad \text{as } z \rightarrow \infty \tag{3.14}$$

where $p_\infty(t)$ is real. Equivalently,

$$f(z, t) \sim \frac{p_\infty(t)}{4}z + O(1/z) \quad \text{as } z \rightarrow \infty. \tag{3.15}$$

The presence of an irrotational straining flow at infinity also implies that

$$g'(z, t) \sim \beta(t)z + \frac{m}{2\pi z} + O\left(\frac{1}{z^3}\right) \quad \text{as } z \rightarrow \infty, \tag{3.16}$$

where $\beta(t)$ is the strain rate and $m(t)$ is the rate of change of the total area of the two bubbles. Notice that the right-hand sides of (3.15) and (3.16) do not contain any $O(1)$ constants because $f(z, t)$ and $g'(z, t)$ are odd functions of z by (3.8).

4. Conformal mappings

Consider the conformal map $z(\zeta, t)$ of the region \mathcal{R} in the ζ -plane, defined by

$$\mathcal{R} \equiv \{ \zeta : \rho_1(t) < |\zeta| < 1, \text{Im}[\zeta] > 0 \},$$

into the first-quadrant region exterior of the upper-right half-bubble $D_R^+(t) \equiv D(t) \cap \{ \text{Re}[z] > 0, \text{Im}[z] > 0 \}$ in the $z = x + iy$ -plane. Figure 2 shows a schematic. To render the mapping unique, we require that $\zeta = 1$ corresponds to the top of the upper bubble on the y -axis and $\zeta = -1$ to the lowest point on this bubble. The remaining degree of freedom in the Riemann-mapping theorem is used by requiring that $\zeta = \pm \rho_1(t)$ corresponds to $z = \infty$ and $z = 0$ respectively, where $\rho_1(t)$ is to be determined. It is clear that $|\zeta| = 1$ corresponds to the upper-right half-bubble, $|\zeta| = \rho_1$ corresponds to the x -axis, while the straight segments in the ζ -plane in the interval $(\rho_1(t), 1)$ and $(-1, -\rho_1(t))$ correspond to the the y -axis segments between ∞ and the top point of the upper bubble and lower point of the upper bubble and $z = 0$; see figure 2. With use of the Schwarz reflection principle (Ablowitz & Fokas 1997), we deduce that $z(\zeta, t)$ maps the annular ring $\rho_1 < |\zeta| < 1$ into the upper-half z -plane region exterior to the upper bubble. In particular, the reflection principle implies

$$\bar{z}(\zeta, t) = -z(\zeta, t). \tag{4.1}$$

In a similar way, a second application of the Schwarz reflection principle (reflecting about $|\zeta| = \rho_1(t)$ this time) and use of the fact that $z(\zeta, t)$ maps $|\zeta| = \rho_1$ onto the real z -axis yields

$$\bar{z}(\zeta, t) = z(\rho_1^2/\zeta, t). \tag{4.2}$$

So $z(\zeta, t)$ maps the doubly connected annular ring $\rho_1^2(t) < |\zeta| < 1$ into the region $D(t)$ outside the two bubbles.

For convenience, introduce the notation $\rho(t) = \rho_1^2(t)$. Combining (4.1) and (4.2), we obtain

$$z(\rho/\zeta, t) = -z(\zeta, t). \tag{4.3}$$

This functional equation corresponds to the fact that if a particular point \hat{z} on the lower bubble corresponds to $\zeta = \rho e^{-iv}$, then the point $\zeta = e^{iv}$ corresponds to the point $-\hat{z}$ on the upper bubble.

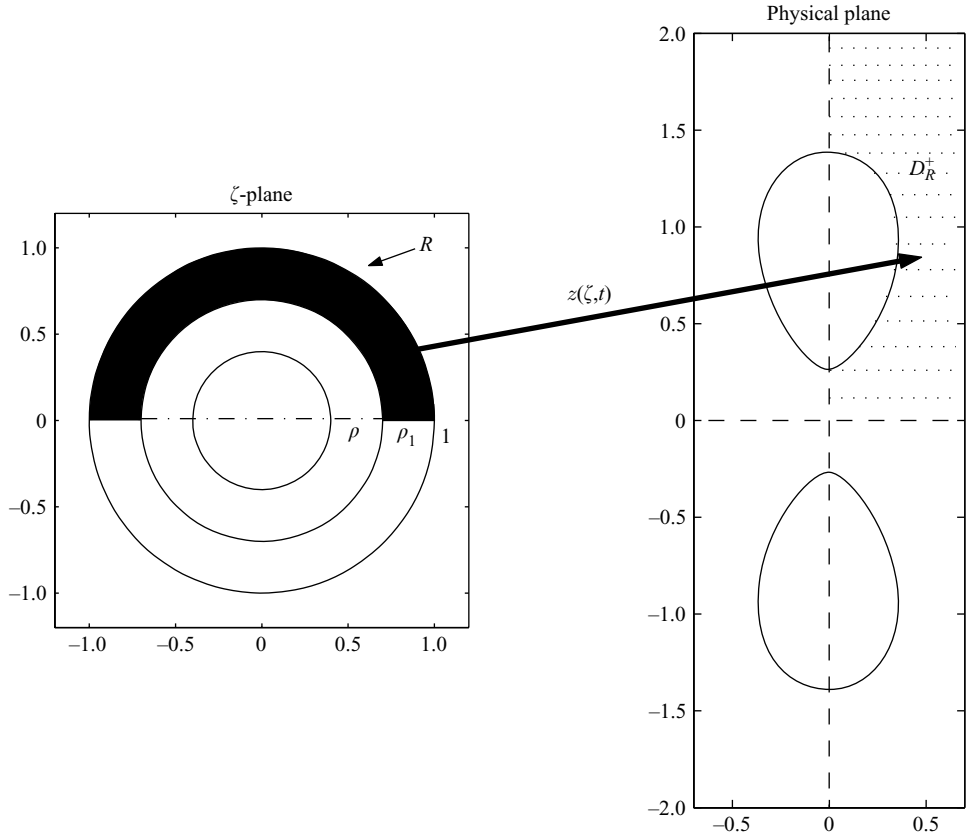


FIGURE 2. Conformal mapping regions. The shaded semi-annulus R in a parametric ζ -plane maps to D_R^+ – the first quadrant exterior to the upper bubble in the physical plane.

The symmetries of the problem imply that the conjugate map $\bar{z}(\zeta, t) \equiv \overline{z(\bar{\zeta}, t)}$ must satisfy

$$\bar{z}(\zeta, t) = -z(\zeta, t). \tag{4.4}$$

Now let

$$z(\zeta, t) = \frac{ia(t)}{\zeta - \sqrt{\rho}(t)} + i\hat{z}(\zeta, t) \tag{4.5}$$

for some real $a(t)$. $\hat{z}(\zeta, t)$ must be analytic everywhere in the annulus $\rho < |\zeta| < 1$ and so has a convergent Laurent expansion there. Let

$$\hat{z}(\zeta, t) = \sum_{n=-\infty}^{\infty} a_n(t)\zeta^n \tag{4.6}$$

where the coefficients $\{a_n\}$ are real in order that (4.4) is satisfied. Then, condition (4.3) translates to

$$\hat{z}(\zeta, t) = -\hat{z}(\rho/\zeta, t) + \frac{a}{\sqrt{\rho}}. \tag{4.7}$$

In particular, this implies

$$a_0 = \frac{a}{2\sqrt{\rho}}, \quad a_{-n} = -\rho^n a_n, \quad n \geq 1. \tag{4.8}$$

When (4.8) is satisfied, it is easy to check that

$$z(-\sqrt{\rho}, t) = 0 \tag{4.9}$$

is automatically satisfied (recall $\zeta = -\rho_1$ corresponds to $z = 0$).

Define the composed functions $\mathcal{F}(\zeta, t)$ and $\mathcal{G}(\zeta, t)$ as follows:

$$\mathcal{F}(\zeta, t) \equiv f(z(\zeta, t), t), \quad \mathcal{G}(\zeta, t) = g'(z(\zeta, t), t). \tag{4.10}$$

In terms of these functions, (3.10) and (3.11) become

$$\mathcal{F}(\zeta, t) + z(\zeta, t) \frac{\overline{\mathcal{F}}_\zeta(\zeta^{-1}, t)}{\overline{z}_\zeta(\zeta^{-1}, t)} + \overline{\mathcal{G}}(\zeta^{-1}, t) = \frac{\zeta z_\zeta(\zeta, t)}{2|z_\zeta(\zeta, t)|} + iC(t) \quad \text{on } |\zeta| = 1, \tag{4.11}$$

$$\mathcal{F}(\zeta, t) + z(\zeta, t) \frac{\overline{\mathcal{F}}_\zeta(\rho^2 \zeta^{-1}, t)}{\overline{z}_\zeta(\rho^2 \zeta^{-1}, t)} + \overline{\mathcal{G}}(\rho^2 \zeta^{-1}, t) = -\frac{\zeta z_\zeta(\zeta, t)}{2\rho|z_\zeta(\zeta, t)|} - iC(t) \quad \text{on } |\zeta| = \rho. \tag{4.12}$$

Note that

$$\overline{\mathcal{F}}(\zeta, t) \equiv \overline{f}(\overline{z}(\zeta, t), t) = f(-z(\zeta, t), t) = -f(z(\zeta, t), t) \equiv -\mathcal{F}(\zeta, t) \tag{4.13}$$

so that

$$\overline{\overline{\mathcal{F}}}(\zeta, t) = -\mathcal{F}(\zeta, t). \tag{4.14}$$

It follows similarly that

$$\overline{\overline{\mathcal{G}}}(\zeta, t) = -\mathcal{G}(\zeta, t). \tag{4.15}$$

Since $f(-z, t) = -f(z, t)$ then using (4.3) it follows that

$$f(-z(\zeta, t), t) = f(z(\rho \zeta^{-1}, t), t) = -f(z(\zeta, t), t) \tag{4.16}$$

so that

$$\mathcal{F}(\rho \zeta^{-1}, t) = -\mathcal{F}(\zeta, t). \tag{4.17}$$

Similarly, given that $g'(-z, t) = -g'(z, t)$ it follows that

$$\mathcal{G}(\rho \zeta^{-1}, t) = -\mathcal{G}(\zeta, t). \tag{4.18}$$

Applying conditions (4.7), (4.14) and (4.15) to (4.11) and (4.12), we can simplify to

$$\mathcal{F}(\zeta, t) + z(\zeta, t) \frac{\overline{\mathcal{F}}_\zeta(\zeta^{-1}, t)}{z_\zeta(\zeta^{-1}, t)} - \mathcal{G}(\zeta^{-1}, t) - iC(t) = \frac{\zeta z_\zeta(\zeta, t)}{2|z_\zeta(\zeta, t)|} \quad \text{on } |\zeta| = 1, \tag{4.19}$$

$$\mathcal{F}(\zeta, t) + z(\zeta, t) \frac{\overline{\mathcal{F}}_\zeta(\rho^2 \zeta^{-1}, t)}{z_\zeta(\rho^2 \zeta^{-1}, t)} - \mathcal{G}(\rho^2 \zeta^{-1}, t) + iC(t) = -\frac{\zeta z_\zeta(\zeta, t)}{2\rho|z_\zeta(\zeta, t)|} \quad \text{on } |\zeta| = \rho. \tag{4.20}$$

Given the far-field asymptotic behaviour (3.15) and (3.16), $\mathcal{F}(\zeta, t)$ and $\mathcal{G}(\zeta, t)$ must have representations of the form

$$\mathcal{F}(\zeta, t) = \frac{iF_\infty}{\zeta - \sqrt{\rho}} + iF(\zeta, t) \quad \text{where } F(\zeta, t) = \sum_{n=-\infty}^{\infty} F_n \zeta^n, \tag{4.21}$$

$$\mathcal{G}(\zeta, t) = \frac{iG_\infty}{\zeta - \sqrt{\rho}} + iG(\zeta, t) \quad \text{where } G(\zeta, t) = \sum_{n=-\infty}^{\infty} G_n \zeta^n \tag{4.22}$$

where the Laurent series are convergent everywhere in the annulus $\rho < |\zeta| < 1$ and the coefficients $\{F_n, G_n\}$ are real in order that (4.14) and (4.15) are satisfied. The

conditions (4.17) and (4.18) become

$$F(\zeta, t) = -F(\rho/\zeta, t) + \frac{F_\infty}{\sqrt{\rho}}, \quad G(\zeta, t) = -G(\rho/\zeta, t) + \frac{G_\infty}{\sqrt{\rho}}. \quad (4.23)$$

This implies the following relations:

$$\left. \begin{aligned} F_0 &= \frac{F_\infty}{2\sqrt{\rho}}, & F_{-n} &= -\rho^n F_n, & n &\geq 1, \\ G_0 &= \frac{G_\infty}{2\sqrt{\rho}}, & G_{-n} &= -\rho^n G_n, & n &\geq 1. \end{aligned} \right\} \quad (4.24)$$

When (4.24) is satisfied, the conditions $\mathcal{F}(-\sqrt{\rho}, t) = 0$ and $\mathcal{G}(-\sqrt{\rho}, t) = 0$ (corresponding to $f(0, t) = 0$ and $g'(0, t) = 0$) are automatically satisfied.

On use of (4.5), the asymptotic conditions (3.15) and (3.16) for large z translate into conditions

$$F_\infty = \frac{a}{4}p_\infty, \quad G_\infty = \beta(t)a, \quad \frac{m}{2\pi} = -aG_\zeta(\sqrt{\rho}, t) + G_\infty \hat{z}_\zeta(\sqrt{\rho}, t). \quad (4.25)$$

On use of (3.16) and (4.5) in an asymptotic expansion near $\zeta = \sqrt{\rho}$, besides (4.25) we apparently obtain the extra condition $\beta \hat{z}_\zeta(\sqrt{\rho}, t) = G(\sqrt{\rho}, t)$. However, this is not independent of (4.7), (4.23) and (4.25) since they imply $\hat{z}_\zeta(\sqrt{\rho}, t) = a/(2\sqrt{\rho})$ and $G(\sqrt{\rho}, t) = G_\infty/(2\sqrt{\rho})$.

Equations (4.19), (4.20), (4.24) and (4.25) determine coefficients $\{F_n, G_n\}$, C and G_∞ in terms of the specified m and β at each instant of time for any given values of the conformal mapping parameters a , ρ and $\{a_n\}$. Note that, since the bubble pressure has been fixed to be zero, it should be expected on physical grounds that one can either choose to externally specify m , in which case p_∞ (and hence F_∞) will be determined by the solution or, alternatively, to externally specify p_∞ (hence F_∞) in which case m will be determined by the solution. Both choices will be made in the calculations to follow in order to model different physical scenarios.

4.1. Kinematic condition

The kinematic condition is used to time-advance the interface. In complex notation, condition (2.4) becomes

$$\text{Im} [(z_t - (u + iv))\bar{z}_s] = 0. \quad (4.26)$$

We can therefore write

$$\text{Re} \left[\frac{z_t + 2\mathcal{F}(\zeta, t)}{\zeta z_\zeta} \right] = \begin{cases} \frac{1}{2|z_\zeta|} + \text{Re} \left[\frac{iC}{\zeta z_\zeta} \right] & \text{on } |\zeta| = 1, \\ -\frac{1}{2\rho|z_\zeta|} - \text{Re} \left[\frac{iC}{\zeta z_\zeta} \right] - \frac{\dot{\rho}}{\rho} & \text{on } |\zeta| = \rho(t), \end{cases} \quad (4.27)$$

where we have used the fact that

$$z_s = \frac{i\zeta z_\zeta}{|z_\zeta|} \quad \text{on } |\zeta| = 1 \quad (4.28)$$

and

$$z_s = -\frac{i\zeta z_\zeta}{\rho|z_\zeta|} \quad \text{on } |\zeta| = \rho(t). \quad (4.29)$$

The term in square brackets on the left-hand side of (4.27) leads to an equation of the form

$$z_t + 2\mathcal{F}(\zeta, t) = \zeta z_\zeta I(\zeta, t) \quad (4.30)$$

where $I(\zeta, t)$ is analytic in the annulus $\rho < |\zeta| < 1$ and determined by using the right-hand side of (4.27) as boundary data on $\text{Re}[I]$ on $|\zeta|=1$ and $|\zeta|=\rho$. An integral representation for $I(\zeta, t)$ is given in Appendix A. For numerical purposes, however, it is more convenient and efficient to use a Laurent series representation, as described below.

To compute $I(\zeta, t)$, we first determine the Laurent expansion coefficients $\{d_n\}$ of

$$\frac{1}{2|z_\zeta|} + \text{Re} \left[\frac{iC}{\zeta z_\zeta} \right] = \sum_{-\infty}^{\infty} d_n \zeta^n \quad \text{on } |\zeta| = 1. \tag{4.31}$$

On use of (4.3) and the fact that $z(\rho e^{-iv}) = -\overline{z(\rho e^{iv})}$ it follows that

$$-\frac{1}{2\rho|z_\zeta(\rho e^{iv})|} - \text{Re} \left[\frac{iC}{[\zeta z_\zeta](\rho e^{iv})} \right] = -\sum_{-\infty}^{\infty} d_n e^{inv}. \tag{4.32}$$

Hence, in order that the average of the data on $|\zeta|=1$ given on the right-hand side of (4.27) equals the average of the data given on $|\zeta|=\rho$, we require

$$d_0 = -d_0 - \frac{\dot{\rho}}{\rho} \tag{4.33}$$

which yields the following equation for $\dot{\rho}$:

$$\dot{\rho} = -2\rho d_0. \tag{4.34}$$

This is equivalent to the condition

$$\oint_{|\zeta|=1} \frac{d\zeta}{\zeta} \left(\frac{1}{2|z_\zeta|} + \text{Re} \left[\frac{iC}{\zeta z_\zeta} \right] \right) = \oint_{|\zeta|=\rho} \frac{d\zeta}{\zeta} \left(-\frac{1}{2\rho|z_\zeta|} - \text{Re} \left[\frac{iC}{\zeta z_\zeta} \right] - \frac{\dot{\rho}}{\rho} \right). \tag{4.35}$$

To determine $I(\zeta, t)$ we write it as the Laurent expansion

$$I(\zeta, t) = \sum_{-\infty}^{\infty} I_n \zeta^n. \tag{4.36}$$

Now, since $\text{Re}[I]$ on the boundary $\zeta = e^{iv}$ and $\zeta = \rho e^{iv}$, given by the right-hand side of (4.27), is an even function of v from symmetry of bubble shapes about the imaginary axis, it follows that I_n must be real. Thus,

$$\text{Re}[I(\zeta, t)] = \frac{1}{2}I(\zeta, t) + \frac{1}{2}I(\zeta^{-1}, t) = \sum_{-\infty}^{\infty} d_n \zeta^n \quad \text{on } |\zeta| = 1 \tag{4.37}$$

and on use of (4.32),

$$\text{Re}[I(\zeta, t)] = \frac{1}{2}I(\zeta, t) + \frac{1}{2}I(\rho^2 \zeta^{-1}, t) = -\frac{\dot{\rho}}{\rho} - \sum_{-\infty}^{\infty} d_n \left(\frac{\zeta}{\rho} \right)^n \quad \text{on } |\zeta| = \rho. \tag{4.38}$$

Comparison of coefficients implies

$$\left. \begin{aligned} I_n &= 2 \left(\frac{1 + \rho^n}{1 - \rho^{2n}} \right) d_n, & n \geq 1, \\ I_0 &= d_0, \\ I_{-n} &= - \left(\frac{2\rho^n}{1 - \rho^n} \right) d_n, & n \geq 1. \end{aligned} \right\} \tag{4.39}$$

Although the above relations between I_n (or I_{-n}) and d_n hold for $n \leq -1$ as well, they will not be used in the numerical algorithm because such calculations will be unstable for large n since $\rho < 1$. Once $I(\zeta, t)$ is known explicitly, we can advance the coefficients $a_n(t)$ in the Laurent series of \hat{z} in time by noting that (4.30) implies

$$\hat{z}_t(\zeta, t) = \zeta \hat{z}_\zeta(\zeta, t) I(\zeta, t) - \frac{a\zeta I(\zeta, t)}{(\zeta - \sqrt{\rho})^2} - \frac{\dot{a}}{\zeta - \sqrt{\rho}} - \frac{\dot{\rho}a}{2\sqrt{\rho}(\zeta - \sqrt{\rho})^2} - \frac{2F_\infty}{\zeta - \sqrt{\rho}} - 2F(\zeta, t). \tag{4.40}$$

In order for \hat{z} to be singularity-free at $\sqrt{\rho}$, we must require that the apparent poles on the right-hand side of (4.40) at that point cancel out. This implies

$$\frac{\dot{\rho}}{2\sqrt{\rho}} = -\sqrt{\rho}I(\sqrt{\rho}, t), \quad \text{or} \quad \frac{d}{dt}\sqrt{\rho} = -\sqrt{\rho}I(\sqrt{\rho}, t), \tag{4.41}$$

$$\dot{a} + 2F_\infty = -aI(\sqrt{\rho}, t) - a\sqrt{\rho}I_\zeta(\sqrt{\rho}, t). \tag{4.42}$$

While (4.35) and (4.41) are two different equations for $\dot{\rho}$ they are equivalent (one implies the other) once the symmetry of the domain is exploited. Justification for this is given in Appendix B. Equation (4.42) relates F_∞ (and therefore p_∞) to conformal mapping parameters and C .

Using the above relations, it follows that (4.40) may be rewritten as

$$\begin{aligned} \hat{z}_t(\zeta, t) = \zeta \hat{z}_\zeta(\zeta, t) I(\zeta, t) - \frac{a\zeta I(\zeta, t) - a\sqrt{\rho}I(\sqrt{\rho}, t)}{(\zeta - \sqrt{\rho})^2} \\ + \frac{aI(\sqrt{\rho}, t) + a\sqrt{\rho}I_\zeta(\sqrt{\rho}, t)}{\zeta - \sqrt{\rho}} - 2F(\zeta, t). \end{aligned} \tag{4.43}$$

By considering coefficients of ζ^n for $n = 1, 2, \dots$ in the Laurent series expansion of both left- and right-hand side of (4.43) on $|\zeta| = 1$, we obtain equations for the evolution of $\{a_n(t) | n \geq 1\}$. The negative coefficients $\{a_n | n = -N, \dots, -1\}$ then follow from (4.8). An equation to determine a is given, in principle, by (4.42) and once a is known, a_0 follows from (4.8). However, in practice, it is found to be more convenient to update a using the equation connecting the rate of change of area to m , i.e.

$$\frac{d\mathcal{A}}{dt} = \frac{m}{2} \tag{4.44}$$

where \mathcal{A} is the area of each bubble. Using contour integration, the representation

$$\mathcal{A}(t) = -\frac{1}{2i} \oint_{|\zeta|=1} \bar{z}(\zeta^{-1}, t) z_\zeta(\zeta, t) d\zeta \tag{4.45}$$

yields a quadratic expression for a in terms of the updated conformal-mapping parameters and the updated area. This quadratic equation can be solved explicitly for a .

It should be clear that we have made maximal use of symmetry in devising this numerical scheme. This is in order to optimize its performance. If required, however, the same general approach can also be used to study the case of two arbitrary bubbles having no geometrical symmetries.

5. Exact solutions

In this section we catalogue all known exact solutions to the two-bubble problem, including some new time-evolving ones that we have identified. All of these can be conveniently stated in terms of the conformal mapping formulation already presented.

It is clear that two steady circular bubbles in a quiescent flow is a solution of the problem. While this is a trivial case, it is helpful to see the form of this solution within the complex-variable formulation of § 3 and § 4. When $C(t) = 0$ we have found that there exists a class of time-evolving exact solutions. These are described in § 5.2. Finally, in § 5.3, we review a class of exact solutions to the problem of two steady bubbles in a nonlinear ambient flow recently found by Crowdy (2002). Conveniently, it turns out that the latter steady solutions provide appropriate initial conditions for the new class of unsteady solutions of § 5.2. Some illustrative calculations of the exact solutions of § 5.2 using these initial conditions are given in § 5.4.

5.1. Two circular bubbles in quiescent flow

Consider the case of quiescent flow exterior to two exactly circular bubbles of unit radius. The conformal map from $\rho < |\zeta| < 1$ to the exterior of the two bubbles must be a Möbius map. Using the fact that we know $\zeta = \sqrt{\rho}$ maps to infinity while $\zeta = -\sqrt{\rho}$ maps to the origin this map must be

$$z(\zeta) = iR(\rho) \left(\frac{\zeta + \sqrt{\rho}}{\zeta - \sqrt{\rho}} \right) = iR(\rho) \left(1 + \frac{2\sqrt{\rho}}{\zeta - \sqrt{\rho}} \right) \tag{5.1}$$

where $R(\rho)$ is chosen so that each bubble radius is 1, i.e. $z(+1) - z(-1) = 2i$, resulting in

$$R(\rho) = \frac{1 - \rho}{2\sqrt{\rho}}. \tag{5.2}$$

Thus,

$$z_\zeta(\zeta) = -\frac{2i\sqrt{\rho}R(\rho)}{(\zeta - \sqrt{\rho})^2}. \tag{5.3}$$

The solution for $f(z)$ and $g(z)$ must be

$$f(z) = \frac{p_\infty}{4}z, \quad g(z) = 0. \tag{5.4}$$

This gives zero velocity everywhere and the required far-field pressure. Therefore

$$F(\zeta) = \frac{p_\infty}{4}z(\zeta). \tag{5.5}$$

The stress condition on bubble 1 is

$$f(z) + z\bar{f}'(\bar{z}) + \bar{g}'(\bar{z}) = -\frac{iz_s}{2} + \mathcal{A}_1 \tag{5.6}$$

while, on bubble 2,

$$f(z) + z\bar{f}'(\bar{z}) + \bar{g}'(\bar{z}) = -\frac{iz_s}{2} + \mathcal{A}_2. \tag{5.7}$$

On bubble 1,

$$z_s = \frac{i\zeta z_\zeta}{|z_\zeta|} \tag{5.8}$$

while on bubble 2,

$$z_s = -\frac{i\zeta z_\zeta}{\rho|z_\zeta|}. \tag{5.9}$$

Equation (5.6) therefore takes the form

$$\frac{p_\infty}{2} z(\zeta) = \frac{\zeta z_\zeta}{2|z_\zeta|} + \mathcal{A}_1 \tag{5.10}$$

while (5.7) becomes

$$\frac{p_\infty}{2} z(\zeta) = -\frac{\zeta z_\zeta}{2\rho|z_\zeta|} + \mathcal{A}_2. \tag{5.11}$$

But, using (5.3), on bubble 1

$$|z_\zeta| = \frac{2\sqrt{\rho}R(\rho)\zeta}{(\zeta - \sqrt{\rho})(1 - \sqrt{\rho}\zeta)} \tag{5.12}$$

while on bubble 2,

$$|z_\zeta| = \frac{2\sqrt{\rho}R(\rho)\zeta}{(\zeta - \sqrt{\rho})(\rho^2 - \sqrt{\rho}\zeta)}. \tag{5.13}$$

Combining all this and substituting into (5.6) and (5.7), yields

$$\frac{ip_\infty R(\rho)}{2} \left(1 + \frac{2\sqrt{\rho}}{\zeta - \sqrt{\rho}}\right) - \mathcal{A}_1 = \frac{i\sqrt{\rho}}{2} - \frac{i(1 - \rho)}{2(\zeta - \sqrt{\rho})} \tag{5.14}$$

and

$$\frac{ip_\infty R(\rho)}{2} \left(1 + \frac{2\sqrt{\rho}}{\zeta - \sqrt{\rho}}\right) - \mathcal{A}_2 = -\frac{i}{2\sqrt{\rho}} - \frac{i(1 - \rho)}{2(\zeta - \sqrt{\rho})} \tag{5.15}$$

Thus, we must have

$$\left. \begin{aligned} \mathcal{A}_1 &= -\frac{i}{4} \left(\sqrt{\rho} + \frac{1}{\sqrt{\rho}} \right), \\ \mathcal{A}_2 &= \frac{i}{4} \left(\sqrt{\rho} + \frac{1}{\sqrt{\rho}} \right), \\ p_\infty &= -1. \end{aligned} \right\} \tag{5.16}$$

The last result also follows from the fact that pressure inside the bubble is 0, while curvature and surface tension are normalized to 1. Note also that $\overline{\mathcal{A}}_1 = \mathcal{A}_2$ and that they are both purely imaginary as predicted earlier. This exact solution can be used as a check on the numerical calculation of the Goursat functions \mathcal{F} and \mathcal{G} .

5.2. Time-evolving exact solutions when $C(t) = 0$

The results to be presented now are motivated by the natural question: can the exact solutions for a single bubble in an ambient Stokes flow (Antanovskii 1994*a*; Tanveer & Vasconcelos 1995) be generalized to the case of two interacting bubbles? Our investigations reveal that, in general, the answer is negative. However, we have found that a special class of exact solutions does exist. Specifically, when $C(t) = 0$, the evolution equations admit a class of time-evolving solutions that can be described in terms of closed-form mathematical formulae. The solutions are of limited physical applicability, however, since the condition that $C(t) = 0$ imposes a constraint on the bubble area evolution for given strain rate $\beta(t)$. This means that the area evolution of the bubbles cannot be specified. However, the solutions are worth reporting since they have mathematical significance: they provide a non-trivial check on the numerical code. For fixed $\beta(t)$, they are found to correspond to shrinking bubbles. Thus, they can at least provide insights into bubbles with shrinking area as might occur when the gas in the bubble dissolves in the ambient fluid.

It can be proved (see Appendix C) that if $C(t)=0$ and if the initial conformal map is such that $z(\rho^2\zeta, 0) = z(\zeta, 0)$ then it retains that this property later in time, i.e.

$$z(\zeta, t) = z(\rho^2\zeta, t). \tag{5.17}$$

Thus $z(\zeta, t)$ remains a doubly periodic function in the variable $\log \zeta$ with periods $2 \log \rho$ and $2\pi i$ if it is so initially.

Further, in a manner similar to Tanveer & Vasconcelos (1995), it can be shown (see Appendix C) that if $C(t)=0$ then the equation for the analytically continued $z(\zeta, t)$ in the region $1 < |\zeta| < \rho^{-1}$ is given by

$$z_t(\zeta, t) = q_1(\zeta, t)z_\zeta(\zeta, t) + q_2(\zeta, t)z(\zeta, t) + q_3(\zeta, t) \tag{5.18}$$

where

$$\left. \begin{aligned} q_1(\zeta, t) &= \zeta I(\zeta, t), \\ q_2(\zeta, t) &= 2 \frac{\overline{\mathcal{F}}_\zeta(\zeta^{-1}, t)}{\overline{z}_\zeta(\zeta^{-1}, t)}, \\ q_3(\zeta, t) &= 2\overline{\mathcal{G}}(\zeta^{-1}, t) \end{aligned} \right\} \tag{5.19}$$

where we borrow the notation from Tanveer & Vasconcelos (1995) to emphasize the similarity in the analytical arguments here and there. Note that all the coefficient functions $q_j(\zeta, t)$, $j = 1, 2, 3$ are analytic for $1 < |\zeta| < \rho^{-1}$, except that at $\zeta = \rho^{-1/2}$, q_3 has a simple pole. Thus, (5.18) has the form of a first-order linear partial differential equation for $z(\zeta, t)$, with coefficients that are analytic for $1 < |\zeta| < \rho^{-1}$, except for the forcing term q_3 that has in general a simple pole at $\rho^{-1/2}$. Since $I(\zeta^{-1}, t) = -I(\zeta, t)$, it follows that $(d/dt)\rho^{-1/2}$ calculated from (4.41) matches the characteristic speed $-q_1(\rho^{-1/2}, t)$; hence the only singularity of $z(\zeta, t)$ generated by the pole in the forcing term q_3 in $1 < |\zeta| < \rho^{-1}$ is a simple pole, also at $\rho^{-1/2}$.

Thus, if $z(\zeta, 0)$ is initially meromorphic in this annulus, it will remain so under evolution. The only pole in the region $\rho \leq |\zeta| \leq 1$ can be at $\zeta = \sqrt{\rho}$, corresponding to $z = \infty$ in the physical domain D . So, in the annular region $\rho \leq |\zeta| < 1/\rho$, $z(\zeta, t)$ is meromorphic.

A function $z(\zeta, 0)$ satisfying $z(\rho^2\zeta, 0) = z(\zeta, 0)$ and which is meromorphic in the annulus $\rho < |\zeta| < \rho^{-1}$ is called a *loxodromic function* (Valiron 1947). Moreover, $\rho < |\zeta| < \rho^{-1}$ is a fundamental annulus for such a function so it is completely determined, up to a constant, by the strengths and locations of its singularities in this annulus. The preceding analysis shows that initial conformal maps that are loxodromic functions remain loxodromic functions under evolution. To analyse this class of solutions, it only remains to find a representation of the loxodromic functions relevant to the symmetric two-bubble problem.

Consider the class of conformal maps $z(\zeta, t)$ given by

$$z(\zeta, t) = iR(t) \left[\frac{P(-\zeta\rho^{-1/2}; \rho)P(-\zeta\rho^{1/2}; \rho)}{P(\zeta\rho^{-1/2}; \rho)P(\zeta\rho^{1/2}; \rho)} \right] L(\zeta, \eta_0, -1; \rho) \left(\prod_{j=1}^N L(\zeta, \eta_j, \zeta_j; \rho) \right) \tag{5.20}$$

where

$$P(\zeta; \rho) = (1 - \zeta) \prod_{k=1}^{\infty} (1 - \rho^{2k}\zeta)(1 - \rho^{2k}\zeta^{-1}), \tag{5.21}$$

and

$$L(\zeta, \eta_j, \zeta_j; \rho) = \frac{P(\zeta \rho^{1/2} \eta_j; \rho) P(\zeta \rho^{1/2} \eta_j^{-1}; \rho)}{P(\zeta \rho^{1/2} \zeta_j; \rho) P(\zeta \rho^{1/2} \zeta_j^{-1}; \rho)}. \tag{5.22}$$

The parameters $R(t)$ and $\eta_0(t)$ are real while the parameters $\{\zeta_j, \eta_j | j = 1, \dots, N\}$ can be generally complex with the understanding that, if any of them are not purely real, then another L -function with parameters given by their complex conjugates must be included in the product in (5.20). For example, if ζ_1 is complex then the product in (5.20) must include the term $L(\zeta, \eta_1, \zeta_1; \rho) L(\zeta, \bar{\eta}_1, \bar{\zeta}_1; \rho)$ in order that $z(\zeta, t)$ satisfies the condition (4.4).

Using the definition (5.21), it is easy to establish the following properties of $P(\zeta; \rho)$ and $L(\zeta, \eta_j, \zeta_j; \rho)$:

$$\left. \begin{aligned} P(\zeta^{-1}; \rho) &= P(\rho^2 \zeta; \rho) = -\zeta^{-1} P(\zeta; \rho); \\ L(\rho^2 \zeta, \eta_j, \zeta_j; \rho) &= L(\zeta, \eta_j, \zeta_j; \rho) = L(\rho \zeta^{-1}, \eta_j, \zeta_j; \rho). \end{aligned} \right\} \tag{5.23}$$

Using (5.23), it is easy to check that $z(\zeta, t)$ given in (5.20) satisfies (5.17) and (4.3).

Inspection of the map (5.20) shows that it has poles at

$$\{\rho^{-1/2} \zeta_j, \rho^{-1/2} \zeta_j^{-1} | j = 1, \dots, N\} \tag{5.24}$$

and these are initially chosen in the domain $1 < |\zeta| < \rho^{-1}$ and must remain in that annular region as long as a solution exists. This is because the only way they can escape this annulus is through $|\zeta| = 1$ or $|\zeta| = \rho^{-1}$. There cannot be any pole singularity on $|\zeta| = 1$ or $|\zeta| = \rho$ as these correspond to the two bubble boundaries where no pole is allowed. From the loxodromic property $z(\rho^2 \zeta, t) = z(\zeta, t)$, a pole is ruled out on $|\zeta| = \rho^{-1}$ as well. The map (5.20) has a pole at $-\rho^{-1/2}$ in the annular region $1 < |\zeta| < \rho^{-1}$. It is clear that that $\bar{z}(\zeta^{-1}, t)$ will have poles at $\rho^{1/2} \zeta_j^{\pm 1}$ for $j = 1, \dots, N$ and at $\zeta = -\sqrt{\rho}$, all in the annular region $\rho < |\zeta| < 1$.

Furthermore, the map $z(\zeta, t)$ has corresponding zeros at

$$\{\rho^{-1/2} \eta_j, \rho^{-1/2} \eta_j^{-1} | j = 1, \dots, N\}. \tag{5.25}$$

and at η_0 , all of which are in $1 < |\zeta| < \rho^{-1}$. The only zero in $\rho \leq |\zeta| \leq 1$ can be at $\zeta = -\sqrt{\rho}$ (which maps to $z = 0$ in the physical domain) since $z(\zeta, t)$ is univalent in that domain.

To determine all the parameters in the exact solution, we need to determine the evolution of these poles and zeros, as well as $R(t)$. To do so, note that if $\mathcal{F}(\zeta, t)$ is eliminated from (4.11) using (4.30), the resulting equation can be written for $C = 0$ as

$$\frac{d}{dt} (\bar{z}(\zeta^{-1}, t) z_\zeta(\zeta, t)) = 2\mathcal{G}(\zeta, t) z_\zeta(\zeta, t) + \frac{d}{d\zeta} (\zeta z_\zeta(\zeta, t) \bar{z}(\zeta^{-1}, t) I(\zeta, t)). \tag{5.26}$$

On integration around a small closed contour \mathcal{C}_{ζ_p} encircling a pole ζ_p of $\bar{z}(\zeta^{-1}, t)$ other than $\zeta = \sqrt{\rho}$, we obtain

$$\frac{d}{dt} \left\{ \oint_{\mathcal{C}_{\zeta_p}} \bar{z}(\zeta^{-1}, t) z_\zeta(\zeta, t) d\zeta \right\} = 0. \tag{5.27}$$

Thus, the residues of $\bar{z}(\zeta^{-1}, t) z_\zeta$ at ζ_p , for every pole of $\bar{z}(\zeta^{-1}, t)$ in the annular region $\rho < |\zeta| < 1$, except $\zeta = \sqrt{\rho}$, are preserved in time.

It is also clear from (5.26) that the evolution equation for any pole ζ_p of $\bar{z}(\zeta^{-1}, t)$ in the annulus $\rho < |\zeta| < 1$ is

$$\frac{d}{dt}\zeta_p = -\zeta_p I(\zeta_p, t), \tag{5.28}$$

as can be determined by a local expansion near $\zeta = \zeta_p$ and equating coefficients of double poles on both sides of the equation. The function $I(\zeta, t)$ can be evaluated using the integral formula given in Appendix A. While (5.28) can be thought of as providing equations to update the pole locations $\rho^{1/2}\zeta_j^{\pm 1}$ and at $\zeta = -\sqrt{\rho}$ (noting that the latter is equivalent to (4.35)), the residue invariance in (5.27) can be thought of as constraints to determine the zeros at $\{\rho^{1/2}\eta_j^{\pm 1} | j = 1, \dots, N\}$, as well as at η_0 . We need one more equation for the evolution of scale parameter $R(t)$ in (5.20). This is obtained by using (5.18) and obtaining an equation for the residue $i\hat{a}$ of z at $\rho^{-1/2}$, where it has a pole, induced by pole of $\mathcal{G}(\zeta^{-1}, t)$ and combining it with (4.42) to eliminate F_∞ to obtain

$$\frac{d}{dt}(a\hat{a}) = \frac{2\beta a^2}{\rho} - 2a\hat{a}\rho^{1/2}I_\zeta(\rho^{1/2}, t). \tag{5.29}$$

\hat{a} and a can be completely determined in terms of the conformal-mapping parameters appearing in (5.20). Hence (5.29) can be thought of as the final equation to determine the remaining parameter $R(t)$. Note that there is no freedom left to insist that the area evolves in accordance to (4.44); rather, this equation determines $m(t)$ as part of the solution. Thus, at the same time as the requirement $C(t) = 0$ leads to exact solutions, it also leads to this constraint on them.

Finally, it should be mentioned that it is also possible to find a class of exact solutions for any number of rotationally symmetric bubbles in an ambient straining flow with the same rotational symmetry. However, these also correspond to a class of solutions in which $m(t)$ cannot be externally specified.

5.3. Two steady bubbles in a nonlinear ambient flow

The flows of interest in this paper involve two bubbles in a linear ambient flow. It is worth pointing out that Crowdy (2002) has identified a class of exact solutions for two steady bubbles in an ambient nonlinear flow typical of that generated at the centre of a four-roller mill. Such a flow corresponds to $f(z)$ and $g(z)$ having a nonlinear large- z asymptotic behaviour of the form

$$\left. \begin{aligned} f(z) &\sim f_3 z^3 + f_1 z + O(z^{-1}), \\ g(z) &\sim g_4 z^4 + g_2 z^2 + O(1) \end{aligned} \right\} \tag{5.30}$$

for some parameters f_3, f_1, g_4 and g_2 . The far-field flow conditions treated in the present paper are linear corresponding to

$$f_3 = g_4 = 0 \tag{5.31}$$

in (5.30). The steady solutions of Crowdy (2002) are given by conformal maps from the annulus $\rho < |\zeta| < 1$ of the form

$$z(\zeta) = \left[\frac{P(-\zeta\sqrt{\rho^{-1}}, \rho)P(-\zeta\sqrt{\rho}, \rho)}{P(\zeta\sqrt{\rho^{-1}}, \rho)P(\zeta\sqrt{\rho}, \rho)} \right] \left(R_1 \frac{P(i\zeta\sqrt{\rho}, \rho)P(-i\zeta\sqrt{\rho}, \rho)}{P(-\zeta\sqrt{\rho}, \rho)P(\zeta\sqrt{\rho}, \rho)} + R_2 \right) \tag{5.32}$$

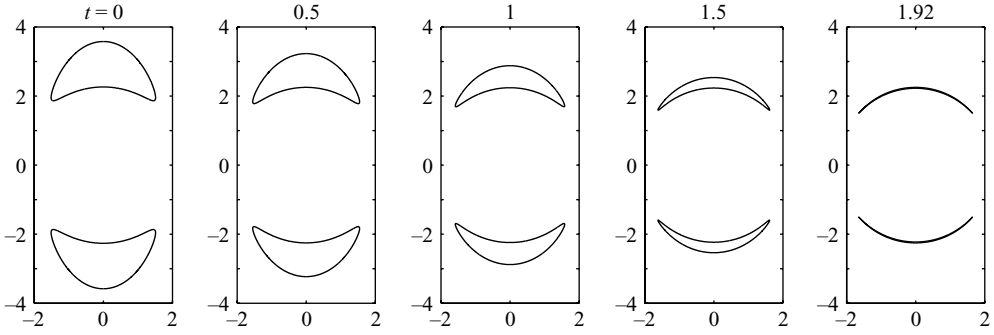


FIGURE 3. The evolution of the exact solution with zero surface tension and $\beta = 0.1$. The bubbles shrink to zero area in the form of two curvilinear slits.

where R_1 and R_2 are real constants. It turns out that the function (5.32) can alternatively be written as

$$z(\zeta, 0) = iR \left[\frac{P(-\zeta \sqrt{\rho}^{-1}; \rho) P(-\zeta \sqrt{\rho}; \rho)}{P(\zeta \sqrt{\rho}^{-1}; \rho) P(\zeta \sqrt{\rho}; \rho)} \right] L(\zeta, \eta_0, -1; \rho) \quad (5.33)$$

which is the simplest non-trivial case of the general maps (5.20). Appendix D indicates how the map (5.32) is related to the form (5.33). This convenient fact means that the steady bubble configurations found in Crowdy (2002) can be used as initial conditions for the following time-dependent calculations thereby obviating the need to search the (ρ, R_1, R_2) -parameter space for univalent maps.

The class of exact solutions found in Crowdy (2002) also requires a constant of integration to vanish, this condition being entirely analogous to the $C(t) = 0$ condition (required for exact solutions) arising in the present analysis. In the steady bubble problem of Crowdy (2002) the consequence is that not all four of the parameters f_3, f_1, g_4 and g_2 defining the far-field ambient flow (5.30) can be independently specified, only three of them. Crowdy (2002) chose to specify the most singular terms f_3, g_4 and the area of the bubble. The values of f_1 and g_2 yielding an exact solution are then determined by the solution itself. In analogy with the results here, it is expected that more general (non-exact) solutions for two steady bubbles can be found when the integration constant is not assumed to vanish.

5.4. Examples of exact solutions involving shrinking bubbles

Here we shall present some examples of the exact solutions discussed in §5.2. In all calculations to follow, the initial condition is given by (5.32) with $\rho = 0.05$, $R_1 = 4.1105$ and $R_2 = -1.4387$. This leads to bubbles each having area π and corresponding to the $\rho = 0.05$, $R_2/R_1 = -0.35$ equilibrium solution shown in figure 7 of Crowdy (2002).

First, we compare the two extreme cases of two-bubble evolution driven purely by the imposed straining flow with zero surface tension and the opposite case of flow driven purely by surface tension with no imposed straining flow. Figures 3 and 4 show these two scenarios. In figure 3 the exact solution is shown to yield collapse of the bubbles to zero area in the form of two curvilinear slits. A similar collapse to a slit has been observed before by Tanveer & Vasconcelos (1995) in the case of a single elliptical bubble shrinking at a fixed rate. In contrast, in figure 4, the solution again leads to shrinkage of the two bubbles but here they both vanish at two isolated points. When both surface tension and an imposed strain are present, the physical problem has two time scales: one associated with surface tension, the other associated

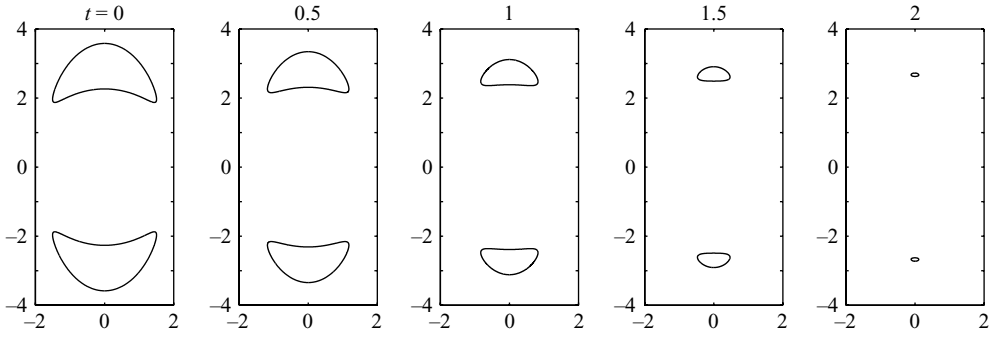


FIGURE 4. The evolution given by the exact solution driven purely by surface tension with $\beta = 0$. The bubbles shrink to zero area at a point.

with the imposed strain rate. The capillary number β measures the ratio of these two time scales. In general, the exact solutions reveal a competition between the two time scales: the bubbles shrink to zero area in the form of a slit if β is sufficiently large and to a single point if β is sufficiently small. If the strain is too strong, there is insufficient time for the bubble to become circular under the effects of surface tension before it collapses to a slit. In their investigations of a slender three-dimensional bubble in a straining flow, Howell & Siegel (2004) also find evidence of the same competition between surface tension and an imposed strain. They notice that an appropriately modulated extensional flow can stabilize a slender jet against pinch-off and can instead lead to cross-sections that become infinitely elongated.

6. Numerical simulations

In this section we present numerical calculations illustrating the possible behaviour of two bubbles in Stokes flow for some cases of interest for which $C(t) \neq 0$. To perform simulations using the scheme of §4.1, the Laurent expansions for \hat{z} , F and G are truncated so that only the terms $\{\zeta^j | j = -N, \dots, N\}$ are included. The algorithm proceeds in two parts: first the Goursat functions F , G and $C(t)$ must be determined for the current conformal mapping parameters a , a_0 , $\{a_{\pm 1}, \dots, a_{\pm N}\}$ and ρ . The second part of the algorithm is to use the Goursat functions F , G and $C(t)$ to update the conformal mapping parameters using the kinematic condition.

Consider the first part of the algorithm. When β and m together with the conformal mapping parameters are considered known, there are $4N + 5$ unknowns to be determined:

$$\{F_j | j = -N, \dots, N\}, \{G_j | j = -N, \dots, N\}, G_\infty, F_\infty, C. \tag{6.1}$$

$2N + 1$ equations come from the truncated Laurent expansion of (4.19), $2N + 2$ equations are given by (4.24), while (4.25) provides two more equations. Note, that because of assumed symmetry, the other stress condition (4.20) is redundant and need not be used at all.

Now consider the second part of the algorithm. Once F_j , G_j , $C(t)$, F_∞ , G_∞ and $C(t)$ are known, and given the conformal mapping parameters a , a_0 , $a_{\pm 1}, \dots, a_{\pm N}$ and ρ , we calculate the Laurent series coefficients $\{I_j | j = -N, \dots, N\}$ for $I(\zeta, t)$ after evaluating $\{d_j | j = -N, \dots, N\}$. We then use only coefficients of $\{\zeta^j | j = 1, \dots, N\}$ in the Laurent series of both sides of (4.43), along with (4.41) and (4.44) to obtain a complete set of ordinary differential equations for a_1, \dots, a_N , ρ and a . Once these are determined, the parameters a_0 and $\{a_{-n} | n = 1, \dots, N\}$ are given by relations (4.8).

If $C(t)=0$, we consider $m(t)$ as an unknown instead of $C(t)$ in the first part of the algorithm. The rest of the algorithm is the same as before.

If $p_\infty=0$, we consider $C(t)$, along with m as unknown in the first part of the algorithm with the rest of the algorithm being the same as before.

All Laurent expansion coefficients are computed using fast Fourier transforms taken at order \mathcal{N} where, typically, we take $\mathcal{N}=16N$ to avoid aliasing errors. The order N of the truncation is chosen to suit the problem. The system of ordinary differential equations is integrated using an explicit fourth-order Runge–Kutta method.

First, as a non-trivial check on the numerical code, we compared a calculation to that given by the class of time-dependent exact solutions derived earlier both in the case of zero and non-zero surface tension. A superposition of the numerical computation with the exact solution in each case revealed them to be indistinguishable. The calculation of the coefficients of $I(\zeta, t)$ using (4.39) was checked using the integral formula given in Appendix A.

6.1. Shrinking bubbles driven purely by surface tension

The exact solutions considered in §5.4 involve shrinking bubbles but the pressure at infinity is not externally specifiable. Shrinking bubbles which close up purely under the effects of surface tension (i.e. $p_\infty=0$) have been considered in detail by Hopper (1990) who found that an isolated circular pore shrinks to zero area at $t_* = 2$. The shrinkage of compressible bubbles (or ‘pores’) in slow viscous flows is of relevance to the problem of viscous sintering (Brinker & Scherer 1990) where an initial compact of touching cylinders (or spheres, in three dimensions) are brought into contact and coalesce under the effects of surface tension. In the late stages of sintering, the compact consists of a contiguous region of fluid containing a distribution of shrinking pores. When all the pores have disappeared, the compact is said to be fully densified. It is important, in order to optimize industrial sinter cycles, to be able to accurately predict the time to full densification. The first theoretical step is to consider simple ‘unit problems’. Hopper (1991) went on to study the closure of elliptical and hypotrochoidal pores. Tanveer & Vasconcelos (1995) have also investigated the properties of shrinking bubbles in Stokes flows.

As an extension to these investigations, it is natural to examine the effect on pore shrinkage of the interaction with neighbouring pores. The simplest scenario is to consider just two identical initially circular pores and to examine how the shrinkage times of one pore is affected by the presence of the other. To study this numerically we therefore impose the condition that

$$F_\infty = 0, \quad G_\infty = 0, \quad (6.2)$$

so that there is no strain flow (i.e. $\beta=0$) and the ambient pressure p_∞ is the same as that in the bubbles (i.e. equal to zero). The flow is then driven purely by surface tension effects. As a result, the rate of change of bubble area (or, equivalently, m) will now be determined by the solution.

Figure 5 shows the evolution, as computed by the numerical code, for initially circular pores given by (5.1). By increasing the value of $\rho(0)$ the pores initially get closer together. When $\rho(0)=0.05$, the effect of the neighbouring pore is slight and each pore shrinks via a sequence of near-circular shapes. As $\rho(0)$ increases so that the pores are initially closer together, the shrinking pores are seen to adopt ellipse-like shapes elongated in the vertical direction and with their centroids gradually moving together. The shrinkage time t_* as the pores start off closer together is found to decrease compared to the isolated case: the effect of the presence of the other pore is to slightly decrease the shrinkage time to zero area. This result is consistent with

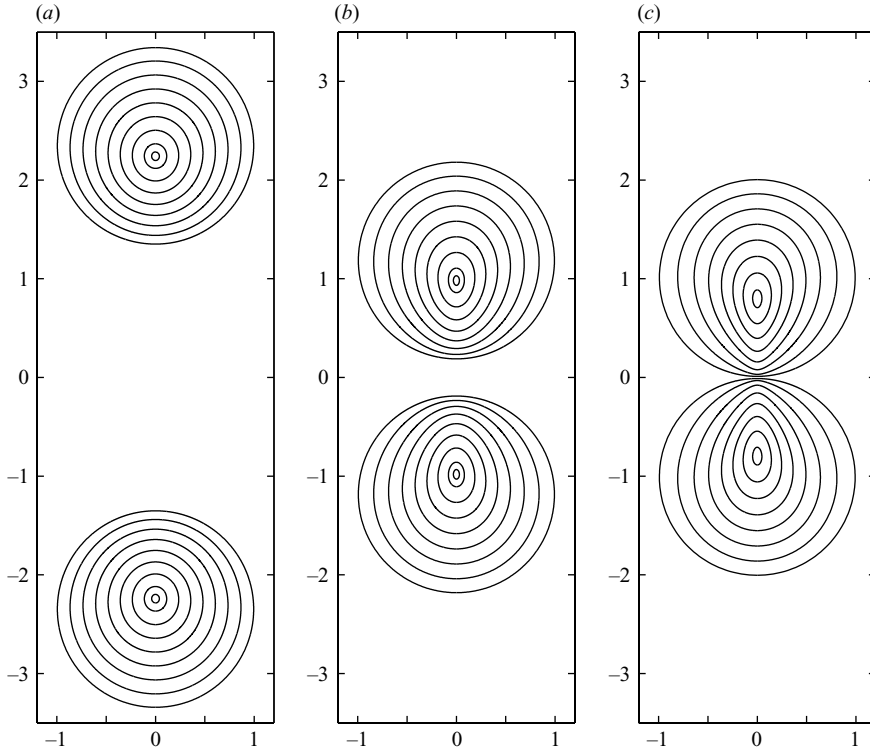


FIGURE 5. Pore closure, driven purely by surface tension, for pores at different initial separations: (a) $\rho(0)=0.05$, (b) 0.3 and (c) 0.75. Here $\beta=0$. The pores are shown at intervals of 0.25 with the final times shown in the figures ((a) to (c)) being $t=1.95, 1.88$ and 1.75 . Note the elongation of the pores in the vertical direction and the downward motion of the pore centroids.

that obtained in the case of a singly periodic row of pores by Crowdy (2004). In the latter work, a simple ‘elliptical pore model’ for the evolution of an interacting collection of compressible pores is proposed based on an asymptotic separation of the full problem into a set of ‘inner’ and ‘outer’ problems. The idea of the model is general and can be applied here. The model results in a simple closed system of nonlinear ordinary differential equations for the evolution of the pair of shrinking pores under the assumption that they are ellipses. The evolution of the upper pore is modelled by a following time-dependent conformal map from a unit η -circle, i.e.

$$z(\eta, t) = ic(t) + \frac{\alpha(t)}{\eta} + \beta(t)\eta \tag{6.3}$$

where

$$\left. \begin{aligned} \dot{\alpha} &= -\alpha \tilde{I}(0, \alpha, \beta), \\ \dot{\beta} &= -\tilde{I}(0, \alpha, \beta) \left(\frac{\alpha^2 \beta - \beta^3 + 2c_1 \beta + \alpha^3}{\alpha^2 - \beta^2 + 2c_1 + \alpha \beta} \right), \\ c^2 &= \frac{\alpha^2 - \beta^2}{2}, \\ c_1 &= \frac{1 + \rho(0)^2}{4\rho(0)}, \end{aligned} \right\} \tag{6.4}$$

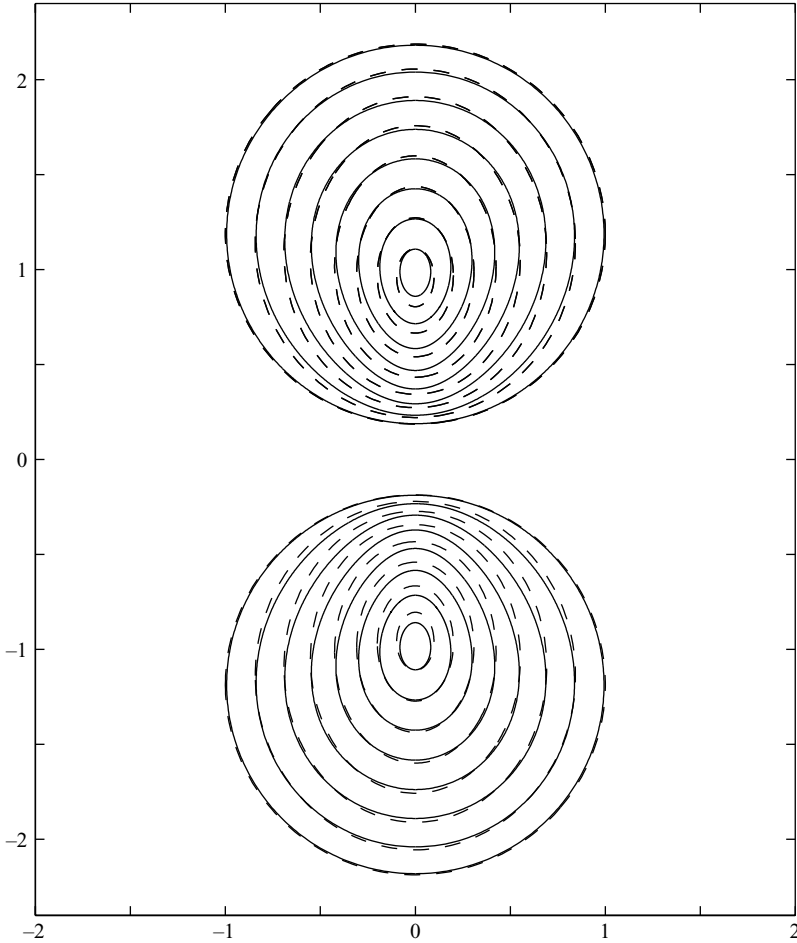


FIGURE 6. Comparison of the numerical simulation of pore closure with the elliptical pore model. The figure shows pore closure driven purely by surface tension with $\rho(0) = 0.3$, $\beta = 0$. The solid lines are the results given by the full numerical simulation, the dashed lines are the results given by the elliptical pore model. Times shown are $t = 0, (0.25), 1.75$.

and where

$$\tilde{I}(0, \alpha, \beta) = \frac{1}{4\pi i} \oint_{|\eta|=1} \frac{d\eta}{\eta} \frac{1}{|z_\eta(\eta, t)|}. \quad (6.5)$$

Appendix E gives details of the derivation of these model equations. They successfully predict the qualitative features already observed: the elongation of the pores in the vertical direction and the downward vertical velocity of the pore centroids. For purposes of qualitative comparison, the results obtained by integrating these model equations have been superposed on the numerical results displayed in figure 6 in the case $\rho(0) = 0.3$. This initial value of ρ is chosen so that the pores are not so far apart that interaction effects between the pores are insignificant but not so close together as to invalidate the assumptions underlying the elliptical pore model. Agreement is found to be very good. The model tends to slightly overestimate the time t_* for the bubble to shrink to area 10^{-3} , yielding $t_* = 1.96$ compared to the value of $t_* = 1.91$ given by the full numerical simulation.

The numerical code copes well with bubbles that are initially very close together as can be seen from the calculation with $\rho(0)=0.75$ in figure 5. The results of a number of calculations reveal that the shrinkage time t_* is a slowly decreasing function of the initial separation of the pores. For the initial condition $\rho(0)=0.75$ so that the initial separation between the bubbles is just 0.02, we find $t_* \approx 1.83$. Thus, the presence of another identical pore can decrease the pore shrinkage time by up to 9%.

A physical discussion of this behaviour can be offered. The presence of two symmetric bubbles forces the existence, at all times in the evolution, of a stagnation point at the origin. The fluid velocities in the central region near this stagnation point between the two bubbles are therefore necessarily small. This leads to an effective ‘pinning’ of the regions of the free surface nearest to the origin. The increased immobility of the free surface associated with this pinning mechanism reduces the effects of surface tension there. This leads to the net displacement of the centroid of each bubble towards the origin and explains the net elongation of the bubbles in the vertical direction. One might suspect, since a small region of the free surface is ‘pinned’ and its motion thereby inhibited, that the net time for shrinkage of the bubble will be increased as a result. This is not the case, as we have seen. The presence of a second bubble, while pinning down a small region of the free surface, in fact induces an anisotropy in the overall surface curvature (via the aforementioned elongation in the y -direction) that leads to a slight overall acceleration of the global shrinkage compared to an isolated bubble. The vertical elongation of the pore serves to enhance the surface tension effects in the vicinity of free surface region that is ‘pinned’ and eventually counteracts the pinning mechanism. This observation is interesting since it contrasts with the case of an initially circular bubble placed near a wall – a problem recently investigated by Crowdy & Duchemin (2005). They find that the presence of the no-slip surface greatly increases the pore shrinkage times owing to a ‘pinning’ effect similar to that just described. Since the wall presents a whole stagnation line in the flow, its pinning effect is clearly much stronger than that produced by the single stagnation point in the two-bubble problem.

6.2. Evolution of constant-area bubbles

It is of interest to examine what happens to two bubbles forced together by a straining flow when they are taken to be incompressible. Such matters are of relevance to the study of two-bubble coalescence (see e.g. Yang *et al.* 2001). We focus here on the role of surface tension in a head-on collision induced by the ambient straining flow. Calculations are performed with $N=256$ and a time step of 10^{-3} . Figure 7(a) shows the case of two initially circular bubbles, with zero surface tension, in an ambient straining flow with $\beta=0.5$. The initial conformal map is (5.1) with $\rho(0)=0.35$. As time evolves, each bubble becomes elongated in the horizontal direction with a thin lubrication layer forming between the bubbles. By $t=1.5$ it is found that each bubble has formed two points of very high curvature at the outermost points from the origin. Each bubble develops a shape that is reminiscent of the single ‘pointed drops’ observed by Taylor (1934) in his experiments in a four-roller mill and studied subsequently, using complex-variable methods, by Antanovskii (1996) and Siegel (2000). Since our model includes no physical mechanism (e.g. a disjoining pressure associated with van der Waals forces) for the bubbles to coalesce as the film drainage between the bubbles occurs, we expect the finite-time formation of two cusps on each of the bubble boundaries thereby leading to breakdown of the mathematical solution.

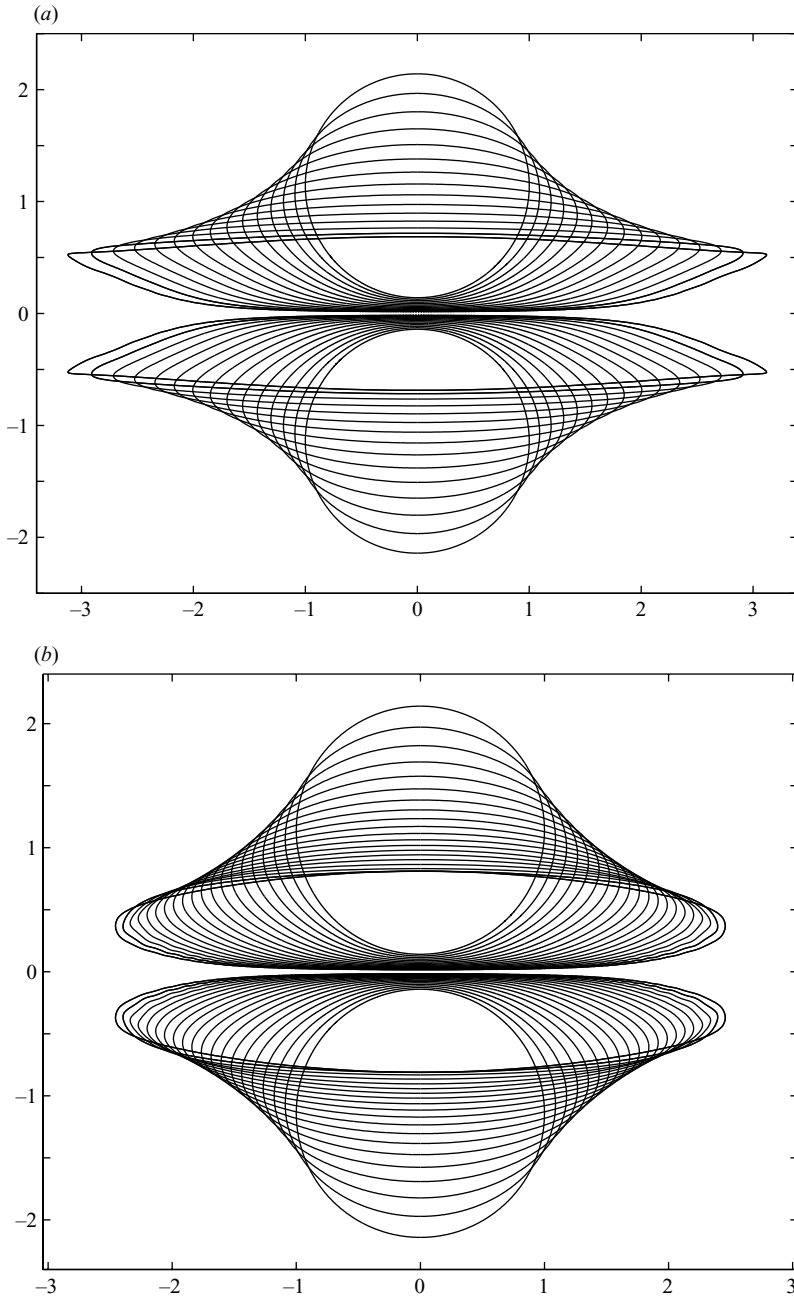


FIGURE 7. The regularizing effect of surface tension when two bubbles are forced together by a straining flow. Evolution with (a) zero and (b) non-zero surface tension. $\rho(0) = 0.35$, $\beta = 0.5$. The area of each bubble is fixed to be π . Times shown are (a) $t = 0, (0.1), 1.5$ and (b) $t = 0, (0.1), 1.9$. In both cases, a thin lubrication layer forms between the bubbles. In the case of zero surface tension, the mathematical solution appears to be approaching breakdown via the formation of two cusps on each bubble. This cusp formation is arrested by capillary effects.

On the other hand, figure 7(b) shows the evolution of the same initial condition when surface tension is present. The effect of surface tension is to regularize the free-surface evolution and appears to arrest the formation of the high-curvature regions.

The solution can be continued well beyond the time of breakdown of the zero surface tension case and figure 4 shows the simulation up to $t=2$. The two bubbles become continually pressed together and a more extended lubrication layer (than in the zero surface tension case) now has time to form between the two bubbles. It is difficult to continue the calculations much beyond $t=2$ because the system becomes very stiff as the bubbles draw closer together and the lubrication layer becomes more extended.

7. Conclusion

In this paper a number of analytical and numerical results for the planar two-bubble problem in Stokes flow have been presented.

Our most significant finding is mathematical: to answer the natural question of whether the large number of exact solutions available in the case of a single bubble carry over to the multi-bubble problem. Our studies here of the two-bubble problem show that, in general, the answer appears to be in the negative even though special classes of exact solution do exist! While we make no claim that the exact solutions we have identified are the only ones possible, we believe the existence of more general exact solutions, for example those corresponding to non-zero $C(t)$, to be unlikely. It should also be pointed out that imposing the condition $C(t)=0$ does not appear to imply that the solutions must correspond to symmetric bubbles: it is therefore conceivable that classes of non-symmetric exact solutions exist. In any case the overall conclusion is that, while the single-bubble problem appears to admit broad classes of exact solution – indeed, the class of initial single-bubble shapes found in Tanveer & Vasconcelos (1995) for which exact solutions exist can approximate arbitrary initial shapes to any degree of accuracy – the presence of multiple bubbles appears to generally destroy the analytical structure responsible for exact solutions. We believe it is important to point out this (albeit disappointing) circumstance. We have not found any physical interpretation for the non-existence of exact solutions for constant-area bubbles in the multi-bubble case; it appears to be a purely mathematical obstruction.

We have examined the extent to which analytical progress (in the form of exact solutions) can be made, and devised a numerical method based on conformal mappings for the general case when exact solutions are not available. To summarize our results:

(a) A special class of time-evolving exact solutions has been found in the case $C(t)=0$. They are the natural analogues of the well-known exact solutions in the single-bubble case. For a fixed strain rate β , they give rise to shrinking bubble solutions. They reveal that a competition between external strain and surface tension can lead to shrinkage either to a slit or a point.

(b) We have presented a novel numerical spectral method based on Laurent series expansions of a conformal mapping from an annulus. The method facilitates calculation of the evolution of bubbles even when they are very close together (and if combined with implicit time-integration methods, we expect the method to be even better). These methods can be extended to the more general case of non-symmetric bubbles and even to the case of greater numbers of bubbles.

(c) We have presented a numerical study of the interaction effects of a neighbouring pore on the shrinkage times of some given pore closing up purely under the effects of surface tension. Despite a local ‘pinning’ of the free surface, the presence of a neighbouring pore can lead to a slight decrease in the overall pore shrinkage time. The numerically computed evolution in this case has been compared with a recently proposed analytical ‘elliptical pore model’ of pore shrinkage.

(d) The effect of surface tension on two plane bubbles forced together by an ambient straining flow has been investigated numerically. Surface tension regularizes the incipient formation of high-curvature regions in the unregularized problem, allowing the formation of extended lubrication layers between the two bubbles and arresting a suspected breakdown of solutions via cusp formation in the unregularized problem.

D. G. C. acknowledges financial support from the Engineering and Physical Sciences Research Council in the UK. S. T. was supported in part by the National Science Foundation (NSF-DMS-0103829 and NSF-DMS-0405837). G. L. V. thanks CNPQ and FINEP (Brazilian agencies) for financial support.

Appendix A. Integral formula for $I(\zeta, t)$

This appendix gives an integral formula for the function $I(\zeta, t)$ used in computing the evolution of the exact solutions in §5.2 and §5.4.

When $C(t) = 0$ (the case relevant to the exact solution class) the kinematic condition takes the form

$$\operatorname{Re}[I(\zeta, t)] = \operatorname{Re} \left[\frac{z_t + 2f(z(\zeta, t), t)}{\zeta z_\zeta} \right] = \begin{cases} \frac{1}{2|z_\zeta|} & \text{on } |\zeta| = 1, \\ -\frac{1}{2\rho|z_\zeta|} - \frac{\dot{\rho}}{\rho} & \text{on } |\zeta| = \rho. \end{cases} \tag{A 1}$$

Let

$$K(\zeta, t) = 1 - 2 \frac{\zeta P_\zeta(\zeta)}{P(\zeta)}. \tag{A 2}$$

Provided that the necessary condition (4.35) is satisfied, the integral formula for $I(\zeta, t)$ is

$$I(\zeta, t) = I^+(\zeta, t) - I^-(\zeta, t) + I_c(t) \tag{A 3}$$

where

$$\left. \begin{aligned} I^+(\zeta, t) &= \frac{1}{2\pi i} \oint_{|\zeta|=1} \frac{d\zeta'}{\zeta'} K(\zeta/\zeta') \frac{1}{2|z_\zeta(\zeta', t)|}, \\ I^-(\zeta, t) &= \frac{1}{2\pi i} \oint_{|\zeta|=\rho} \frac{d\zeta'}{\zeta'} K(\zeta/\zeta') \left(-\frac{1}{2\rho|z_\zeta(\zeta', t)|} - \frac{\dot{\rho}}{\rho} \right), \\ I_c(t) &= -\frac{1}{2\pi i} \oint_{|\zeta|=\rho} \frac{d\zeta'}{\zeta'} \left(-\frac{1}{2\rho|z_\zeta(\zeta', t)|} - \frac{\dot{\rho}}{\rho} \right), \end{aligned} \right\} \tag{A 4}$$

where $P(\zeta; \rho)$ is the function defined in (5.21). Using the properties that

$$K(\rho^2\zeta, t) = 2 + K(\zeta, t), \quad K(\zeta^{-1}, t) = -K(\zeta, t), \tag{A 5}$$

it is straightforward to show that

$$I(\zeta^{-1}, t) = -\bar{I}(\zeta, t), \quad I(\rho^2\zeta, t) = I(\zeta, t). \tag{A 6}$$

In classical function theory, the integral formula presented here is the doubly connected generalization of the Poisson integral formula (Ablowitz & Fokas 1997) and is sometimes known as the Villat formula (Akhiezer 1990).

Appendix B. Equivalence of $(d/dt)\sqrt{\rho} = -\sqrt{\rho}I(\sqrt{\rho}, t)$ and (4.35)

We first simplify the expression for $I(\sqrt{\rho}, t)$. This simplification only requires that $\zeta = \rho/\zeta'$ and holds equally for $\zeta = -\sqrt{\rho}$. First, recall the integral formula of Appendix A:

$$I(\zeta, t) = I^+(\zeta, t) - I^-(\zeta, t) + I_c(t).$$

Consider

$$-I^-(\zeta, t) = \frac{1}{4\pi i} \oint_{|\zeta'|=\rho} \frac{d\zeta'}{\zeta'} \left(1 - 2 \frac{\zeta P'(\zeta/\zeta'; \rho)}{\zeta' P(\zeta/\zeta'; \rho)} \right) \left\{ \frac{1}{\rho |z_\zeta(\zeta', t)|} + \frac{2\dot{\rho}}{\rho} \right\}. \tag{B1}$$

On changing variables $\zeta' \mapsto \rho/\zeta'$ and using properties $\zeta \mapsto \rho/\zeta$ (for the point in question), $P(\eta^{-1}, \rho) = -\eta^{-1}P(\eta, \rho)$, $\zeta z_\zeta(\zeta) = \rho/\zeta z_\zeta(\rho\zeta^{-1}, t)$ we obtain

$$-I^-(\zeta, t) = -\frac{1}{4\pi i} \oint_{|\zeta'|=1} \frac{d\zeta'}{\zeta'} \left(1 - 2 \frac{\zeta P'(\zeta/\zeta'; \rho)}{\zeta' P(\zeta/\zeta'; \rho)} \right) \left\{ \frac{1}{|z_\zeta(\zeta', t)|} + \frac{2\dot{\rho}}{\rho} \right\}. \tag{B2}$$

Adding the expressions for $I^+(\zeta, t)$ and $I_c(\zeta, t)$, we obtain

$$I(\zeta, t) = -\frac{2\dot{\rho}}{\rho} \frac{1}{4\pi i} \oint_{|\zeta'|=1} \frac{d\zeta'}{\zeta'} \left(1 - 2 \frac{\zeta P'(\zeta/\zeta'; \rho)}{\zeta' P(\zeta/\zeta'; \rho)} \right) + \frac{1}{4\pi i} \oint_{|\zeta'|=\rho} \frac{d\zeta'}{\zeta'} \left[\frac{1}{\rho |z_\zeta(\zeta', t)|} + \frac{2\dot{\rho}}{\rho} \right]. \tag{B3}$$

However, the steps above leading to the equality of (B1) and (B2) can be repeated without the $1/|z_\zeta|$ term inside the integral. In that case, we obtain

$$\frac{1}{4\pi i} \oint_{|\zeta'|=\rho} \frac{d\zeta'}{\zeta'} \left(1 - 2 \frac{\zeta P'(\zeta/\zeta'; \rho)}{\zeta' P(\zeta/\zeta'; \rho)} \right) = -\frac{1}{4\pi i} \oint_{|\zeta'|=1} \frac{d\zeta'}{\zeta'} \left(1 - 2 \frac{\zeta P'(\zeta/\zeta'; \rho)}{\zeta' P(\zeta/\zeta'; \rho)} \right)$$

On the other hand, from the calculus of residues,

$$\frac{1}{4\pi i} \left[\oint_{|\zeta'|=1} - \oint_{|\zeta'|=\rho} \right] \frac{d\zeta'}{\zeta'} \left(1 - 2 \frac{\zeta P'(\zeta/\zeta'; \rho)}{\zeta' P(\zeta/\zeta'; \rho)} \right) = 1.$$

It then follows that

$$I(\zeta, t) = \frac{1}{4\pi i} \oint_{|\zeta'|=1} \frac{d\zeta'}{\zeta'} \frac{1}{|z_\zeta(\zeta', t)|} = \frac{1}{8\pi i} \left[\oint_{|\zeta'|=1} \frac{d\zeta'}{\zeta'} \frac{1}{|z_\zeta(\zeta', t)|} + \oint_{|\zeta'|=\rho} \frac{d\zeta'}{\zeta'} \frac{1}{\rho |z_\zeta(\zeta', t)|} \right] \tag{B4}$$

On use of (4.35), it follows from the above equation that

$$\frac{d}{dt} \sqrt{\rho} = -\sqrt{\rho}I(\sqrt{\rho}, t).$$

Again, if we assume the above relation, (4.35) follows. So the two relations are equivalent.

Appendix C. Derivation of $z(\rho^2\zeta, t) = z(\zeta, t)$ and (5.18)

The following derivation is the doubly connected generalization of the analysis presented in Tanveer & Vasconcelos (1995) to justify the exact solutions in the simply connected case. A similar argument is given by Crowdy & Tanveer (2004) in their

discussion of the different, but related, problem of viscous fingering in a Hele-Shaw cell when two free surfaces are involved.

First note that equation (4.30), valid for $\rho < |\zeta| < 1$, can be analytically continued into the annulus $1 < |\zeta| < \rho^{-1}$. The result is that for $1 < |\zeta| < \rho^{-1}$,

$$z_t(\zeta, t) + 2\mathcal{F}(\zeta, t) = \zeta I(\zeta, t)z_\zeta(\zeta, t) + \zeta z_\zeta(\zeta, t) \left[\frac{1}{z_\zeta^{1/2}(\zeta, t)\bar{z}_\zeta^{1/2}(\zeta^{-1}, t)} \right] \quad (\text{C } 1)$$

while its continuation into $\rho^2 < |\zeta| < \rho$ is

$$z_t(\zeta, t) + 2\mathcal{F}(\zeta, t) = \zeta I(\zeta, t)z_\zeta(\zeta, t) + \zeta z_\zeta(\zeta, t) \left[-\frac{1}{\rho z_\zeta^{1/2}(\zeta, t)\bar{z}_\zeta^{1/2}(\rho^2\zeta^{-1}, t)} - \frac{2\dot{\rho}}{\rho} \right]. \quad (\text{C } 2)$$

If $1 < |\zeta| < \rho^{-1}$ then $\rho^2 < |\rho^2\zeta| < \rho$ so that letting $\zeta \mapsto \rho^2\zeta$ in (C 2) yields

$$z_t(\rho^2\zeta, t) + 2\mathcal{F}(\rho^2\zeta, t) = \rho^2\zeta I(\rho^2\zeta, t)z_\zeta(\rho^2\zeta, t) - \frac{\rho\zeta z_\zeta^{1/2}(\rho^2\zeta, t)}{\bar{z}_\zeta^{1/2}(\zeta^{-1}, t)} - 2\dot{\rho}\rho\zeta z_\zeta(\rho^2\zeta, t). \quad (\text{C } 3)$$

Now define

$$H(\zeta, t) \equiv z(\zeta, t) - z(\rho^2\zeta, t). \quad (\text{C } 4)$$

Then, subtracting (C 3) from (C 1),

$$H_t(\zeta, t) = z_t(\zeta, t) - z_t(\rho^2\zeta, t) - 2\dot{\rho}\rho\zeta z_\zeta(\rho^2\zeta, t) - 2\mathcal{F}(\zeta, t) + \zeta I(\zeta, t)z_\zeta(\zeta, t) + \frac{\zeta z_\zeta^{1/2}(\zeta, t)}{\bar{z}_\zeta^{1/2}(\zeta^{-1}, t)} + 2\mathcal{F}(\rho^2\zeta, t) - \rho^2\zeta I(\rho^2\zeta, t)z_\zeta(\rho^2\zeta, t) + \frac{\rho\zeta z_\zeta^{1/2}(\rho^2\zeta, t)}{\bar{z}_\zeta^{1/2}(\zeta^{-1}, t)}. \quad (\text{C } 5)$$

The stress condition on $|\zeta| = 1$ takes the form

$$-2\mathcal{F}(\zeta, t) + \frac{\zeta z_\zeta^{1/2}(\zeta, t)}{\bar{z}_\zeta^{1/2}(\zeta^{-1}, t)} = 2\bar{\mathcal{G}}(\zeta^{-1}, t) + 2\frac{\overline{\mathcal{F}}_\zeta(\zeta^{-1}, t)}{\bar{z}_\zeta(\zeta^{-1}, t)}z(\zeta, t) \quad (\text{C } 6)$$

while, on $|\zeta| = \rho$, it takes the form

$$-2\mathcal{F}(\zeta, t) - \frac{\zeta z_\zeta^{1/2}(\zeta, t)}{\rho\bar{z}_\zeta^{1/2}(\rho^2\zeta^{-1}, t)} = 2\bar{\mathcal{G}}(\rho^2\zeta^{-1}, t) + 2\frac{\overline{\mathcal{F}}_\zeta(\rho^2\zeta^{-1}, t)}{\bar{z}_\zeta(\rho^2\zeta^{-1}, t)}z(\zeta, t). \quad (\text{C } 7)$$

Letting $\zeta \mapsto \rho^2\zeta$ in (C 7),

$$-2\mathcal{F}(\rho^2\zeta, t) - \frac{\rho\zeta z_\zeta^{1/2}(\rho^2\zeta, t)}{\bar{z}_\zeta^{1/2}(\zeta^{-1}, t)} = 2\bar{\mathcal{G}}(\zeta^{-1}, t) + 2\frac{\overline{\mathcal{F}}_\zeta(\zeta^{-1}, t)}{\bar{z}_\zeta(\zeta^{-1}, t)}z(\rho^2\zeta, t). \quad (\text{C } 8)$$

Subtracting (C 8) from (C 6) yields

$$-2\mathcal{F}(\zeta, t) + 2\mathcal{F}(\rho^2\zeta, t) + \frac{\zeta z_\zeta^{1/2}(\zeta, t)}{\bar{z}_\zeta^{1/2}(\zeta^{-1}, t)} + \frac{\rho\zeta z_\zeta^{1/2}(\rho^2\zeta, t)}{\bar{z}_\zeta^{1/2}(\zeta^{-1}, t)} = 2\frac{\overline{\mathcal{F}}_\zeta(\zeta^{-1}, t)}{\bar{z}_\zeta(\zeta^{-1}, t)}H(\zeta, t). \quad (\text{C } 9)$$

But the expression on the left-hand side of (C 9) appears on the right-hand side of (C 5). Substituting for this expression, (C 5) becomes

$$H_t(\zeta, t) = 2\frac{\overline{\mathcal{F}}_\zeta(\zeta^{-1}, t)}{\bar{z}_\zeta(\zeta^{-1}, t)}H(\zeta, t) + \zeta I(\zeta, t)z_\zeta(\zeta, t) - \rho^2\zeta I(\rho^2\zeta, t)z_\zeta(\rho^2\zeta, t). \quad (\text{C } 10)$$

However, on use of property (A 6) of the function $I(\zeta, t)$ (see Appendix A) it follows that

$$H_t(\zeta, t) - \zeta I(\zeta, t)H_\zeta(\zeta, t) - 2\frac{\overline{\mathcal{F}}_\zeta(\zeta^{-1}, t)}{\bar{z}_\zeta(\zeta^{-1}, t)}H(\zeta, t) = 0. \tag{C 11}$$

Equation (C 11) has the form of a first-order linear partial differential equation for H with coefficients that are analytic everywhere in the annulus $1 < |\zeta| < \rho^{-1}$. If $H(\zeta, 0) = 0$ then the unique solution is

$$H(\zeta, t) = z(\zeta, t) - z(\rho^2\zeta, t) = 0. \tag{C 12}$$

Thus, $z(\zeta, t)$ remains a doubly periodic function in the variable $\log \zeta$ with periods $2 \log \rho$ and $2\pi i$ if it is so initially.

Note also that substituting the left-hand side of (C 6) into (C 1) yields (5.18) with q_1, q_2 and q_3 given by (5.19).

Appendix D. The steady solutions of Crowdy (2002)

The steady solutions of Crowdy (2002) are given as

$$z(\zeta) = \frac{P_1(-\zeta\sqrt{\rho^{-1}}; \rho)}{P_1(\zeta\sqrt{\rho^{-1}}; \rho)} \left(A \frac{Q_2(\zeta\sqrt{\rho}; \rho)}{P_2(\zeta\sqrt{\rho}; \rho)} + B \frac{P_1(-\zeta\sqrt{\rho}; \rho)}{P_1(\zeta\sqrt{\rho}; \rho)} \right) \tag{D 1}$$

where ρ, A and B are real constants and the connections with the notation of the present paper are

$$\left. \begin{aligned} P_1(\zeta; \rho) &\equiv P(\zeta; \rho), \\ P_2(\zeta; \rho) &\equiv P(\zeta; \rho)P(-\zeta; \rho), \\ Q_2(\zeta; \rho) &\equiv P(i\zeta; \rho)P(-i\zeta; \rho). \end{aligned} \right\} \tag{D 2}$$

Equation (D 1) is a loxodromic function (Valiron 1947). On use of (D 2), (D 1) takes the form

$$z(\zeta) = \left[\frac{P(-\zeta\sqrt{\rho^{-1}}, \rho)P(-\zeta\sqrt{\rho}, \rho)}{P(\zeta\sqrt{\rho^{-1}}, \rho)P(\zeta\sqrt{\rho}, \rho)} \right] \left(A \frac{P(i\zeta\sqrt{\rho}, \rho)P(-i\zeta\sqrt{\rho}, \rho)}{P(-\zeta\sqrt{\rho}, \rho)P(\zeta\sqrt{\rho}, \rho)} + B \right) \tag{D 3}$$

which can be rewritten as

$$z(\zeta) = R \left(\frac{P(-\zeta\sqrt{\rho^{-1}}, \rho)P(-\zeta\sqrt{\rho}, \rho)}{P(\zeta\sqrt{\rho^{-1}}, \rho)P(\zeta\sqrt{\rho}, \rho)} \right) L(\zeta, \eta_0, -1, ; \rho) \tag{D 4}$$

for some real R and η_0 , which is of the form (5.20) (to within a rotation of the configuration by $\pi/2$ since the bubbles in Crowdy (2002) were taken to be centred on the real axis).

Appendix E. The elliptical-pore model equations

Here we derive the evolution equations for the ‘elliptical-pore model’ of the two-bubble system based on the general theory presented in Crowdy (2004). The ‘outer flow’ generated by the shrinking elliptical pores is assumed to be given by two point sinks, each of strength $m < 0$, at positions $\pm ic$. Thus, the outer flow is modelled by

$$u - iv = \frac{m}{2\pi(z - ic)} + \frac{m}{2\pi(z + ic)}. \tag{E 1}$$

Now consider the flow near the pores. By symmetry, it is enough to consider the flow near the pore in the upper-half plane. Letting $z = ic + \mathcal{Z}$ and expanding the outer flow (E 1) in powers of \mathcal{Z} yields

$$u - iv = \frac{m}{2\pi\mathcal{Z}} - \frac{im}{4\pi c} + \frac{m}{2\pi} \frac{\mathcal{Z}}{4c^2} + \dots \quad (\text{E } 2)$$

Ignoring the first term on the right-hand side of (E 2) which simply corresponds to the sink at ic , the second term corresponds to a net velocity of the pore centroid while the third term gives the linear straining flow in which the ellipse sits. The second term yields

$$\dot{c} = \frac{m}{4\pi c}. \quad (\text{E } 3)$$

Now the ‘inner problem’ is to solve for the evolution of a compressible elliptical bubble in an irrotational straining flow with strain rate

$$k(t) = \frac{m(t)}{8\pi c(t)^2} \quad (\text{E } 4)$$

where this far-field behaviour is determined from the linear term in the local expansion (E 2) of the outer flow field. To describe the evolution of the elliptical bubble, introduce a conformal map from a unit η -circle to the exterior of the elliptical bubble, i.e.

$$z(\eta, t) = ic(t) + \frac{\alpha(t)}{\eta} + \beta(t)\eta. \quad (\text{E } 5)$$

The evolution equations for α and β are given in Crowdy (2003a). They are

$$\left. \begin{aligned} \dot{\alpha} &= -\alpha \tilde{I}(0, \alpha, \beta), \\ \dot{\beta} &= -\beta \tilde{I}(0, \alpha, \beta) + 2k(t)\alpha \end{aligned} \right\} \quad (\text{E } 6)$$

where $\tilde{I}(0, \alpha, \beta)$ is defined in (6.5). By conservation of fluid mass, m must equal the rate of change of the area of the ellipse, i.e.

$$m = \frac{d}{dt} (\pi(\alpha^2 - \beta^2)) = 2\pi(\alpha\dot{\alpha} - \beta\dot{\beta}) \quad (\text{E } 7)$$

which is the equation coupling the strain rate $k(t)$ back to the evolution of the parameters $c(t)$, $\alpha(t)$ and $\beta(t)$ and allowing the model system to be closed in a self-consistent way. Substituting (E 7) into (E 3) gives

$$c\dot{c} = \frac{\alpha\dot{\alpha} - \beta\dot{\beta}}{2} \quad (\text{E } 8)$$

which can be integrated immediately to give

$$c^2 = \frac{\alpha^2 - \beta^2}{2} + c_1 \quad (\text{E } 9)$$

where c_1 is some constant. For an initially circular bubble corresponding to the Möbius map (5.1) with $\rho = \rho(0)$ it can be shown that

$$c_1 = \frac{1 + \rho(0)^2}{4\rho(0)}. \quad (\text{E } 10)$$

Combining all these equations results in a closed, consistent model system given by (6.4).

REFERENCES

- ABLOWITZ, M. & FOKAS, A. S. 1997 *Complex Variables*. Cambridge University Press.
- ACRIVOS, A. 1983 The breakup of small drops and bubbles in shear flows. *Ann. NY Acad. Sci.* **404**, 1–11.
- AKHIEZER, N. I. 1990 *Elements of the Theory of Elliptic Functions*. AMS Monographs.
- ANTANOVSKII, L. K. 1994a Quasi-steady deformation of a two-dimensional bubble placed within a potential viscous flow. *Meccanica-J. Ital. Assoc. Theor. Appl. Maths* **29**, 27–42.
- ANTANOVSKII, L. K. 1994b A plane inviscid incompressible bubble placed within a creeping viscous flow: formation of a cusped bubble. *Eur. J. Mech. B* **13**, 491–509.
- ANTANOVSKII, L. K. 1996 Formation of a pointed drop in Taylor's four-roller mill. *J. Fluid Mech.* **327**, 325–341.
- BRINKER, C. J. & SCHERER, G. W. 1990 *Sol-gel Science: The Physics and Chemistry of Sol-gel Processing*. Academic.
- CROWDY, D. G. 2002 Exact solutions for two steady inviscid bubbles in the slow viscous flow generated by a four-roller mill. *J. Engng Maths* **44**, 311–330.
- CROWDY, D. G. 2003a Compressible bubbles in Stokes flow. *J. Fluid Mech.* **476**, 345–356.
- CROWDY, D. G. 2003b Viscous sintering of unimodal and bimodal cylindrical packings with shrinking pores. *Eur. J. Appl. Maths* **14**, 421–445.
- CROWDY, D. G. 2004 An elliptical pore model of late-stage planar viscous sintering. *J. Fluid Mech.* **501**, 251–277.
- CROWDY, D. G. & DUCHEMIN, L. 2005 The effect of solid boundaries on pore shrinkage in Stokes flow. *J. Fluid Mech.* **531**, 359–379.
- CROWDY, D. G. & TANVEER, S. 2004 The effect of finiteness in the Saffman-Taylor viscous fingering problem. *J. Statist. Phys.* **114**, 1501–1536.
- CUMMINGS, L. J. & HOWELL, P. D. 1999 On the evolution of non-axisymmetric viscous fibres with surface tension, inertia and gravity. *J. Fluid Mech.* **389**, 361–389.
- EGGERS, J., LISTER, J. R. & STONE, H. A. 1990 Coalescence of liquid drops. *J. Fluid Mech.* **401**, 293–310.
- HOPPER, R. W. 1990 Plane Stokes flow driven by capillarity on a free surface. *J. Fluid Mech.* **213**, 349–375.
- HOPPER, R. W. 1991 Plane Stokes flow driven by capillarity on a free surface: further developments. *J. Fluid Mech.* **230**, 355–364.
- HOWELL, P. D. & SIEGEL, M. 2004 The evolution of a slender non-axisymmetric drop in an extensional flow. *J. Fluid Mech.* **521**, 155–180.
- KROPINSKI, M. C. A 2002 Numerical methods for multiple inviscid interfaces in creeping flows. *J. Comput. Phys.* **180**, 1–24.
- RALLISON, J. M. 1984 The deformation of small viscous drops and bubbles in shear flows. *Annu. Rev. Fluid Mech.* **16**, 45–66.
- RICHARDSON, S. 1968 Two-dimensional bubbles in slow-viscous flow. *J. Fluid Mech.* **33**, 475–493.
- RICHARDSON, S. 1973 Two-dimensional bubbles in slow-viscous flow. Part 2. *J. Fluid Mech.* **58**, 115–127.
- RICHARDSON, S. 2000 Plane Stokes flow with time-dependent free boundaries in which the fluid region occupies a doubly-connected region. *Eur. J. Appl. Maths* **11**, 249–269.
- SIEGEL, M. 2000 Cusp formation for time-evolving bubbles in two-dimensional Stokes flow. *J. Fluid Mech.* **412**, 227–257.
- STONE, H. A. 1994 Dynamics of drop formation and breakup in viscous fluids. *Annu. Rev. Fluid Mech.* **26**, 65–102.
- TANVEER, S. & VASCONCELOS, G. L. 1995 Time-evolving bubbles in two-dimensional Stokes flow. *J. Fluid Mech.* **301**, 325–344.
- TAYLOR, G. I. 1934 The formation of emulsions in definable fields of flow. *Proc. R. Soc. Lond. A* **146**, 501–523.
- VALIRON, G. 1947 *Cours d'Analyse Mathématique: Théorie des Fonctions*. Masson et Cie, Paris.
- YANG, H., PARK, C. C., HU, Y. T. & LEAL, L. G. 2001 The coalescence of two equal-sized drops in a two-dimensional linear flow. *Phys. Fluids* **13**, 1087–1106.